

Exploring $B \rightarrow \pi\pi, \pi K$ Decays at the High-Precision Frontier

Robert Fleischer ^{a,b} Ruben Jaarsma ^a, Eleftheria Malami ^a and K. Keri Vos ^c

^a*Nikhef, Science Park 105, NL-1098 XG Amsterdam, Netherlands*

^b*Department of Physics and Astronomy, Vrije Universiteit Amsterdam, NL-1081 HV Amsterdam, Netherlands*

^c*Theoretische Physik 1, Naturwissenschaftlich-Technische Fakultät, Universität Siegen, D-57068 Siegen, Germany*

Abstract

The $B \rightarrow \pi\pi, \pi K$ system offers a powerful laboratory to probe strong and weak interactions. Using the isospin symmetry, we determine hadronic $B \rightarrow \pi\pi$ parameters from data where new measurements of direct CP violation in $B_d^0 \rightarrow \pi^0\pi^0$ resolve a discrete ambiguity. With the help of the $SU(3)$ flavour symmetry, the $B \rightarrow \pi\pi$ parameters can be converted into their $B \rightarrow \pi K$ counterparts, thereby allowing us to make predictions of observables. A particularly interesting decay is $B_d^0 \rightarrow \pi^0 K_S$ as it exhibits mixing-induced CP violation. Using an isospin relation, complemented with a robust $SU(3)$ input, we calculate correlations between the direct and mixing-induced CP asymmetries of $B_d^0 \rightarrow \pi^0 K_S$, which are the theoretically cleanest $B \rightarrow \pi K$ probes. Interestingly, they show tensions with respect to the Standard Model. Should this $B \rightarrow \pi K$ puzzle originate from New Physics, electroweak penguins offer an attractive scenario for new particles to enter. We present a strategy to determine the parameters characterising these topologies and obtain the state-of-the-art picture from current data. In the future, this method will allow us to reveal the $B \rightarrow \pi K$ dynamics and to obtain insights into the electroweak penguin sector with unprecedented precision.

Contents

1	Introduction	1
2	The $B \rightarrow \pi\pi$ system	3
2.1	Amplitude structure	3
2.2	Observables and hadronic parameters	4
3	The $B \rightarrow \pi K$ system	7
3.1	Amplitude structure	7
3.2	Determination of the hadronic parameters	9
3.3	Observables and dynamics	13
3.3.1	Branching ratios	13
3.3.2	Colour-suppressed electroweak penguins	13
3.3.3	Direct CP asymmetries and sum rules	14
3.4	Vanishing CP violation in the electroweak penguin sector	15
4	Correlations between CP asymmetries of $B_d^0 \rightarrow \pi^0 K_S$	18
4.1	Preliminaries	18
4.2	Discrete ambiguities	21
4.3	How to resolve the $B \rightarrow \pi K$ puzzle?	22
5	Extracting the electroweak penguin parameters	24
5.1	Preliminaries	24
5.2	Utilizing mixing-induced CP violation in $B_d^0 \rightarrow \pi^0 K_S$	28
6	Conclusions	31

1 Introduction

For decades, the B -meson system has been an exciting playground for theorists and experimentalists to test the flavour- and CP-violating sector of the Standard Model (SM) [1], which is encoded in the Cabibbo–Kobayashi–Maskawa (CKM) matrix [2, 3]. After an era of pioneering measurements at the B factories with the BaBar and Belle experiments as well as the Tevatron, the experimental stage is currently governed by the Large Hadron Collider (LHC) with its dedicated B -decay experiment LHCb. In the near future, Belle II at the KEK Super B Factory will join these explorations, allowing for exciting new opportunities [4], which will be complemented by the LHCb upgrade [5].

In this endeavour, $B \rightarrow \pi K$ channels are a particularly interesting decay class (for a selection of original references, see Refs. [6–15]). These modes are dominated by QCD penguin topologies as the tree contributions are strongly suppressed by the tiny CKM matrix element $|V_{ub}|$. In the case of $B^+ \rightarrow \pi^0 K^+$ and $B_d^0 \rightarrow \pi^0 K^0$, colour-allowed electroweak (EW) penguin topologies enter at the same level as colour-allowed tree amplitudes, contributing $\mathcal{O}(10\%)$ to the decay amplitudes. As an illustration, we show the decay topologies that contribute to the $B_d^0 \rightarrow \pi^0 K^0$ channel in Fig. 1. Since New Physics (NP) may well enter through EW penguins [16–21], these $B \rightarrow \pi K$ modes are especially promising. Examples of specific models are given by NP scenarios with extra Z' bosons [18–21], which are receiving a lot of attention in view of anomalies in rare B -decay data (see Ref. [22] and references therein).

In general, NP contributions are associated with new sources of CP violation that can be probed through CP-violating observables. In this respect, $B_d^0 \rightarrow \pi^0 K_S$ is a particularly interesting decay as it is the only $B \rightarrow \pi K$ mode exhibiting mixing-induced CP violation [23, 24]. This phenomenon emerges from interference between B_d^0 – \bar{B}_d^0 mixing and decay processes of B_d^0 and \bar{B}_d^0 mesons into the $\pi^0 K_S$ final state. As we will demonstrate in this paper, the mixing-induced CP asymmetry of $B_d^0 \rightarrow \pi^0 K_S$ plays an outstanding role for testing the SM with the $B \rightarrow \pi K$ system. This paper complements Refs. [25, 26], where we gave a compact presentation of the main results discussed in detail below.

Analyses of non-leptonic B decays are in general very challenging due to hadronic matrix elements of four-quark operators entering the corresponding low-energy effective Hamiltonians. In the case of the $B \rightarrow \pi K$ decays, the flavour symmetries of strong interactions imply relations between the $B \rightarrow \pi K$ amplitudes and those of the $B \rightarrow \pi\pi, KK$ systems, which allow us to eliminate the hadronic amplitudes or to determine them from experimental data for the latter decays.

In our analysis, we aim at keeping the theoretical assumptions about strong interactions as minimal as possible, and shall use results from QCD factorization (QCDF) to include $SU(3)$ -breaking corrections [12]. A central role is played by an isospin relation between amplitudes of neutral $B \rightarrow \pi K$ decays. Complementing it with an $SU(3)$ input to just fix a certain normalisation, this relation allows us to calculate a correlation between the direct and mixing-induced CP asymmetries of the $B_d^0 \rightarrow \pi^0 K_S$ mode [24]. We find an intriguing tension with the SM, implying either that the current central values of the relevant observables will change in the future or signals of NP contributions which involve in particular new sources of CP violation.

In order to clarify this situation and to reveal the dynamics underlying the EW penguin contributions of the $B \rightarrow \pi K$ decays, we develop a new strategy to determine the corresponding parameters. It utilises again the isospin relation between the neutral $B \rightarrow \pi K$ decays as well as its counterpart for the charged modes. As the experimental

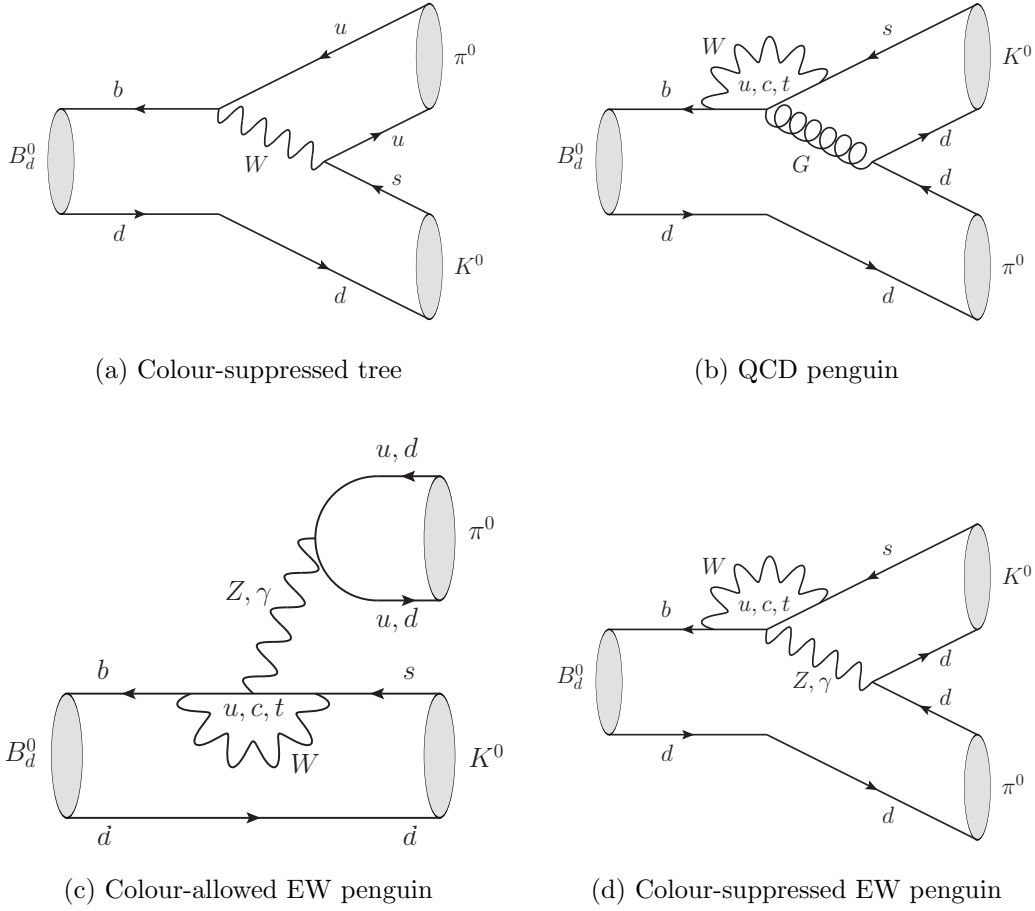


Figure 1: Topologies contributing to the $B_d^0 \rightarrow \pi^0 K^0$ channel.

picture is shaper for the latter case, we perform a detailed analysis of these modes, resulting in the currently most stringent constraints on the EW penguin parameters. In the future, these quantities can be determined with the help of measurements of the mixing-induced CP asymmetry of $B_d^0 \rightarrow \pi^0 K_S$. We illustrate the promising potential of this method by discussing a variety of scenarios. The Belle II experiment offers exciting prospects for future measurements of the CP asymmetries in $B_d^0 \rightarrow \pi^0 K_S$ [4], which will allow us to enter a new territory in terms of precision. Concerning $B \rightarrow \pi K, \pi\pi$ modes with charged pions and kaons in the final states, the LHCb upgrade will also have an important impact for the implementation of the new strategy.

The outline of this paper is as follows: in Section 2, we discuss the hadronic parameters following from the current $B \rightarrow \pi\pi$ data, where an important new ingredient is given by measurements of direct CP violation in $B_d^0 \rightarrow \pi^0\pi^0$. Having these parameters at hand, we apply the $SU(3)$ flavour symmetry to calculate their $B \rightarrow \pi K$ counterparts in Section 3, exploring also the impact of $SU(3)$ -breaking corrections. In Section 4, we utilize the isospin symmetry to calculate correlations between the CP asymmetries of $B_d^0 \rightarrow \pi^0 K_S$ and discuss the intriguing picture following from the current measurements. In Section 5, we present the details of the new method to determine the EW penguin parameters, apply it to the current data and demonstrate that we can match the expected experimental precision in the era of Belle II and the LHC upgrade(s) with the theoretical uncertainties. Finally, we summarize our conclusions in Section 6.

2 The $B \rightarrow \pi\pi$ system

2.1 Amplitude structure

The $B \rightarrow \pi\pi$ system has been studied extensively in Ref. [16]. Here we present an update of the determination of the hadronic parameters from the corresponding data, which we will use as input parameters in the $B \rightarrow \pi K$ analysis. The amplitudes of the charged and neutral $B \rightarrow \pi\pi$ decays satisfy the following isospin relation [27]:

$$\sqrt{2}A(B^+ \rightarrow \pi^+\pi^0) = A(B_d^0 \rightarrow \pi^+\pi^-) + \sqrt{2}A(B_d^0 \rightarrow \pi^0\pi^0), \quad (1)$$

and have contributions from colour-allowed tree (\mathcal{T}), colour-suppressed tree (\mathcal{C}), penguin (\mathcal{P}), exchange (\mathcal{E}), and penguin-annihilation (\mathcal{PA}) topologies. The amplitudes can be parametrised in the following way [16, 17]:

$$\sqrt{2}A(B^+ \rightarrow \pi^+\pi^0) = -\tilde{T}e^{i\gamma}(1 + xe^{i\Delta})(1 + \tilde{q}e^{-i\beta}e^{-i\gamma}) \quad (2)$$

$$A(B_d^0 \rightarrow \pi^-\pi^+) = -\tilde{T}(e^{i\gamma} - de^{i\theta}) \quad (3)$$

$$\sqrt{2}A(B_d^0 \rightarrow \pi^0\pi^0) = P \left[1 + \frac{x}{d}e^{i\gamma}e^{i(\Delta-\theta)} + \tilde{q} \left(\frac{1 + xe^{i\Delta}}{d}e^{-i\theta}e^{-i\beta} \right) \right], \quad (4)$$

where

$$\tilde{T} = \lambda^3 AR_b(\mathcal{T} - \mathcal{P}_{tu} + \mathcal{E} - \mathcal{PA}_{tu}), \quad (5)$$

$$P = \lambda^3 A(\mathcal{P}_t - \mathcal{P}_c). \quad (6)$$

We use the notation \mathcal{P}_{tq} and \mathcal{PA}_{tq} for the difference between penguin and penguin-annihilation topologies with internal t and q quarks, respectively, and introduce

$$de^{i\theta} \equiv -\frac{1}{R_b} \frac{\mathcal{P}_{tc} + \mathcal{PA}_{tc}}{\mathcal{T} - \mathcal{P}_{tu} + \mathcal{E} - \mathcal{PA}_{tu}}, \quad (7)$$

$$xe^{i\Delta} \equiv \frac{\mathcal{C} + \mathcal{P}_{tu} - \mathcal{E} + \mathcal{PA}_{tu}}{\mathcal{T} - \mathcal{P}_{tu} + \mathcal{E} - \mathcal{PA}_{tu}}. \quad (8)$$

For the considerations below, it is interesting to consider also the ratio

$$r_c^{\pi\pi} e^{i\delta_c^{\pi\pi}} \equiv \epsilon R_b \left[\frac{\mathcal{T} + \mathcal{C}}{\mathcal{P}_{tc} + \mathcal{PA}_{tc}} \right] = -\frac{\epsilon}{de^{i\theta}}(1 + xe^{i\Delta}), \quad (9)$$

where

$$\epsilon \equiv \frac{\lambda^2}{1 - \lambda^2} = 0.0535 \pm 0.0002 \quad (10)$$

involves the Wolfenstein parameter $\lambda \equiv |V_{us}| = 0.22543 \pm 0.00042$, and

$$R_b \equiv \left(1 - \frac{\lambda^2}{2} \right) \frac{1}{\lambda} \left| \frac{V_{ub}}{V_{cb}} \right| = 0.390 \pm 0.030 \quad (11)$$

measures one side of the UT. Furthermore, $A \equiv |V_{cb}|/\lambda^2 = 0.8227_{-0.0136}^{+0.0066}$ is another CKM factor [33, 34] (for the numerical values, see Ref. [35]). The UT angle γ can be determined

Mode	$\mathcal{B}r[10^{-6}]$	A_{CP}^f	S_{CP}^f	Ref.
$B_d^0 \rightarrow \pi^+\pi^-$	5.12 ± 0.19	0.31 ± 0.05	-0.66 ± 0.06	[28, 29]
$B_d^0 \rightarrow \pi^0\pi^0$	1.59 ± 0.18	0.33 ± 0.22	–	[30, 31]
$B^+ \rightarrow \pi^+\pi^0$	5.5 ± 0.4	0.03 ± 0.04	–	[28]

Table 1: Overview of the currently available $B \rightarrow \pi\pi$ measurements. Note that the branching ratios are actually CP-averaged quantities.

in a theoretically clean way from pure tree decays of the kind $B \rightarrow D^{(*)}K^{(*)}$ [36, 37] (for an overview, see [38]). In our numerical analyses, we use

$$\gamma = (70 \pm 7)^\circ, \quad (12)$$

which is an average of the experimental results compiled by the CKMfitter [35] and UTfit [39] collaborations and agrees with Ref. [40]. In the future, the uncertainty of the γ determination from pure $B \rightarrow D^{(*)}K^{(*)}$ tree decays can be reduced to the 1° level thanks to Belle II and the LHCb upgrade [4, 5].

In the $B \rightarrow \pi\pi$ system, the EW penguin topologies play a very minor role and are described by

$$\tilde{q} \equiv \left| \frac{P_{EW} + P_{EW}^C}{T + C} \right| \sim 1.3 \times 10^{-2} \left| \frac{V_{td}}{V_{ub}} \right| \sim 3 \times 10^{-2}, \quad (13)$$

where

$$T = \lambda^3 AR_b \mathcal{T}, \quad C = \lambda^3 AR_b \mathcal{C}. \quad (14)$$

For completeness, we have included them in Eqs. (2–4) using the isospin symmetry of the strong interactions [10, 42]. Their effect on the determination of the hadronic parameters d, θ and x, Δ is negligible given the current uncertainties [16]. In the future, these contributions could be taken into account through a more sophisticated analysis.

2.2 Observables and hadronic parameters

In Table 1, we list the $B \rightarrow \pi\pi$ data used in our analysis. Here and in the following considerations, the branching ratios are actually CP-averaged quantities. The branching ratio of $B_d^0 \rightarrow \pi^0\pi^0$ quoted in Table 1 is an average of the BaBar measurement [30]

$$\mathcal{B}r(B_d^0 \rightarrow \pi^0\pi^0) = (1.83 \pm 0.21 \pm 0.13) \times 10^{-6} \quad (15)$$

and the recent Belle result [31]

$$\mathcal{B}r(B_d^0 \rightarrow \pi^0\pi^0) = (1.31 \pm 0.19 \pm 0.18) \times 10^{-6}, \quad (16)$$

following from the procedure by the Particle Data Group (PDG) [28]. Recently, a new LHCb measurement of the CP asymmetries in $B_d^0 \rightarrow \pi^-\pi^+$ came out [32], where values close to the averages in Table 1 were reported.

For the charged B -meson decays, we introduce direct CP asymmetries as

$$A_{\text{CP}}^f \equiv \frac{\Gamma(B^- \rightarrow \bar{f}) - \Gamma(B^+ \rightarrow f)}{\Gamma(B^- \rightarrow \bar{f}) + \Gamma(B^+ \rightarrow f)}. \quad (17)$$

In case of the decay of a neutral B_d^0 meson into a final state that is an eigenstate of the CP operator, we have the following time-dependent decay rate asymmetry:

$$\mathcal{A}_{\text{CP}}(t) \equiv \frac{\Gamma(\bar{B}_d^0(t) \rightarrow f) - \Gamma(B_d^0(t) \rightarrow f)}{\Gamma(\bar{B}_d^0(t) \rightarrow f) + \Gamma(B_d^0(t) \rightarrow f)} = A_{\text{CP}}^f \cos(\Delta M_d t) + S_{\text{CP}}^f \sin(\Delta M_d t), \quad (18)$$

where the time dependence comes from the oscillations between the B_d^0 and \bar{B}_d^0 states, and $\Delta M_d \equiv M_{\text{H}}^{(d)} - M_{\text{L}}^{(d)}$ denotes the mass differences between the ‘‘heavy’’ and ‘‘light’’ B_d mass eigenstates, respectively [43]. The observable A_{CP}^f describes direct CP violation as in Eq. (17), while S_{CP}^f measures mixing-induced CP violation. In Eq. (18), we neglect the decay width difference $\Delta\Gamma_d = (\Gamma_{\text{H}}^{(d)} - \Gamma_{\text{L}}^{(d)})/\Gamma_d = \mathcal{O}(10^{-3})$. First measurements of the direct CP asymmetry of the $B_d^0 \rightarrow \pi^0\pi^0$ channel are available. In Table 1, we quote the average of the BaBar result [30]

$$A_{\text{CP}}^{\pi^0\pi^0} = 0.43 \pm 0.26 \pm 0.05 \quad (19)$$

and the recent Belle measurement [31]

$$A_{\text{CP}}^{\pi^0\pi^0} = 0.14 \pm 0.36 \pm 0.12. \quad (20)$$

Using the parameters in Eqs. (7) and (8), we obtain

$$A_{\text{CP}}^{\pi^-\pi^+} = \frac{2d \sin \theta \sin \gamma}{1 - 2d \cos \theta \cos \gamma + d^2}, \quad (21)$$

$$S_{\text{CP}}^{\pi^-\pi^+} = - \left[\frac{d^2 \sin \phi_d - 2d \cos \theta \sin(\phi_d + \gamma) + \sin(\phi_d + 2\gamma)}{1 - 2d \cos \theta \cos \gamma + d^2} \right] \quad (22)$$

and

$$A_{\text{CP}}^{\pi^0\pi^0} = \frac{-2dx \sin(\theta - \Delta) \sin \gamma}{d^2 + 2dx \cos(\theta - \Delta) \cos \gamma + x^2}, \quad (23)$$

$$S_{\text{CP}}^{\pi^0\pi^0} = - \left[\frac{d^2 \sin \phi_d + 2dx \cos(\theta - \Delta) \sin(\phi_d + \gamma) + x^2 \sin(\phi_d + 2\gamma)}{d^2 + 2dx \cos(\theta - \Delta) \cos \gamma + x^2} \right], \quad (24)$$

where

$$\phi_d = (43.2 \pm 1.8)^\circ \quad (25)$$

denotes the CP-violating B_d^0 - \bar{B}_d^0 mixing phase. The numerical value follows from an analysis of CP violation in $B_d^0 \rightarrow J/\psi K_S$ [28], including corrections from doubly Cabibbo-suppressed penguin effects [44].

Using the value of γ in Eq. (12) and the current experimental values of the CP asymmetries in $B_d^0 \rightarrow \pi^-\pi^+$, we find the following hadronic parameters [40, 41]:

$$d = 0.58 \pm 0.16, \quad \theta = (151.4 \pm 7.6)^\circ. \quad (26)$$

In order to get a handle on x and Δ , it is useful to introduce the ratios

$$R_{+-}^{\pi\pi} \equiv 2 \frac{M_{B^+}}{M_{B_d}} \frac{\Phi(m_\pi/M_{B_d}, m_\pi/M_{B_d})}{\Phi(m_{\pi^0}/M_{B^+}, m_\pi/M_{B^+})} \left[\frac{\mathcal{B}r(B^+ \rightarrow \pi^+\pi^0)}{\mathcal{B}r(B_d^0 \rightarrow \pi^+\pi^-)} \right] \frac{\tau_{B_d^0}}{\tau_{B^+}} \stackrel{\text{exp}}{\equiv} 2.00 \pm 0.16 \quad (27)$$

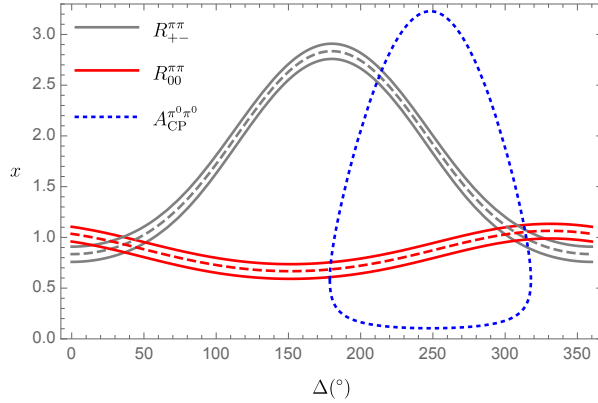


Figure 2: Determination of x and Δ from the current data for the ratios $R_{+-}^{\pi\pi}$ and $R_{00}^{\pi\pi}$. The two-fold ambiguity can be resolved through the direct CP asymmetry $A_{CP}^{\pi^0\pi^0}$, where the current experimental central value results in the dotted blue line.

and

$$R_{00}^{\pi\pi} \equiv 2 \frac{\Phi(m_\pi/M_{B_d}, m_\pi/M_{B_d})}{\Phi(m_{\pi^0}/M_{B_d}, m_{\pi^0}/M_{B_d})} \left[\frac{\mathcal{B}r(B_d^0 \rightarrow \pi^0\pi^0)}{\mathcal{B}r(B_d^0 \rightarrow \pi^+\pi^-)} \right] \stackrel{\text{exp}}{=} 0.621 \pm 0.074, \quad (28)$$

where

$$\Phi(X, Y) = \sqrt{[1 - (X + Y)^2][1 - (X - Y)^2]} \quad (29)$$

is the usual phase-space function. We have used the CP-averaged branching ratios in Table 1 and $\tau_{B^+}/\tau_{B_d^0} = 1.076 \pm 0.004$ [28]. Needless to note, the branching ratios still have large uncertainties, which influence $R_{00}^{\pi\pi}$ accordingly. In terms of the hadronic parameters introduced above, we obtain

$$R_{+-}^{\pi\pi} = \frac{1 + 2x \cos \Delta + x^2}{1 - 2d \cos \theta \cos \gamma + d^2} \quad (30)$$

and

$$R_{00}^{\pi\pi} = \frac{d^2 + 2dx \cos(\Delta - \theta) \cos \gamma + x^2}{1 - 2d \cos \theta \cos \gamma + d^2}, \quad (31)$$

which give

$$x = -\cos \Delta \pm \sqrt{r_\pi R_{+-}^{\pi\pi} - \sin^2 \Delta} \quad (32)$$

and

$$x = -d \cos \gamma \cos(\Delta - \theta) \pm \sqrt{r_\pi R_{00}^{\pi\pi} - (1 - \cos^2(\Delta - \theta))d^2}, \quad (33)$$

respectively, with

$$r_\pi = 1 - 2d \cos \theta \cos \gamma + d^2. \quad (34)$$

Using the current measurements, we illustrate the corresponding contours in Fig. 2. Interestingly, the emerging twofold ambiguity for x and Δ can be resolved through the direct CP asymmetry of the $B_d^0 \rightarrow \pi^0\pi^0$ channel, resulting in

$$x = 1.04 \pm 0.09, \quad \Delta = -(52.3 \pm 19.3)^\circ. \quad (35)$$

In a previous analysis [16], the ambiguity was resolved with the help of the $SU(3)$ flavour symmetry and the $B^\pm \rightarrow \pi^0 K^\pm$ channel, where the unphysical solution would result in

Mode	$\mathcal{B}r[10^{-6}]$	A_{CP}	S_{CP}
$\bar{B}_d^0 \rightarrow \pi^+ K^-$	19.6 ± 0.5	-0.082 ± 0.006	—
$\bar{B}_d^0 \rightarrow \pi^0 \bar{K}^0$	9.9 ± 0.5	0.00 ± 0.13	0.58 ± 0.17
$B^+ \rightarrow \pi^+ K_S$	23.7 ± 0.8	-0.017 ± 0.016	—
$B^+ \rightarrow \pi^0 K^+$	12.9 ± 0.5	0.037 ± 0.021	—

Table 2: Overview of the current measurements in the $B \rightarrow \pi K$ system [28].

a large direct CP asymmetry that is excluded by experimental data. The clean new constraint following from the $A_{\text{CP}}^{\pi^0\pi^0}$ is consistent with these considerations.

Using the parameters determined above, we find the following SM predictions for the CP asymmetries of the $B_d^0 \rightarrow \pi^0\pi^0$ channel:

$$A_{\text{CP}}^{\pi^0\pi^0}|_{\text{SM}} = 0.44 \pm 0.21, \quad S_{\text{CP}}^{\pi^0\pi^0}|_{\text{SM}} = 0.81 \pm 0.32, \quad (36)$$

which depend strongly on the value of $\mathcal{B}r(B_d^0 \rightarrow \pi^0\pi^0)$. In comparison with Ref. [16], the prediction for the mixing-induced CP asymmetry moved up by almost 1σ . The Belle II collaboration expects to reach an uncertainty for the $B_d^0 \rightarrow \pi^0\pi^0$ branching ratio of $\pm 0.03(\text{stat.}) \pm 0.05(\text{syst.})$ [4], whereas the expected uncertainties of the direct and mixing-induced CP asymmetries are ± 0.04 and ± 0.33 , respectively [4].

Finally, we determine the ratio in Eq. (9) as

$$r_c^{\pi\pi} = 0.17 \pm 0.04, \quad \delta_c^{\pi\pi} = (1.9 \pm 7.5)^\circ, \quad (37)$$

where we have used Eqs. (26) and (35). We note that $\delta_c^{\pi\pi}$ takes a remarkably small value, which is driven by the determination of the strong phase Δ . The counterpart of this quantity in the $B \rightarrow \pi K$ system will play an important role in the later discussion. It is interesting to note that the pattern of the values in Eq. (37) is in accordance with the corresponding QCDF predictions [12, 45]. The determination of the hadronic $B \rightarrow \pi\pi$ parameters discussed above is actually clean from the theoretical point of view as it depends only on isospin relations and the experimental values of γ and ϕ_d .

3 The $B \rightarrow \pi K$ system

3.1 Amplitude structure

We now focus on the $B \rightarrow \pi K$ system. The $B^+ \rightarrow \pi^+ K^0$ and $B_d^0 \rightarrow \pi^- K^+$ amplitudes have only colour-suppressed EW penguins, while $B^+ \rightarrow \pi^0 K^+$ and $B_d^0 \rightarrow \pi^0 K^0$ have in addition contributions from colour-allowed EW penguin topologies. The EW penguin contributions are described by the following parameter:

$$qe^{i\phi}e^{i\omega} \equiv - \left(\frac{\hat{P}'_{EW} + \hat{P}'^C_{EW}}{\hat{T}' + \hat{C}'} \right), \quad (38)$$

where ϕ and ω are CP-violating and CP-conserving phases, and \hat{P}'_{EW} (\hat{T}') and \hat{P}'^C_{EW} (\hat{C}') denote colour-allowed and colour-suppressed EW penguin (tree) amplitudes, respectively.

In the SM, the contribution of the EW penguins can be calculated by using the general expressions for the corresponding four-quark operators. The Wilson coefficients of the

EW penguin operators Q_7 and Q_8 are tiny and their contributions can be neglected. The remaining Q_9 and Q_{10} operators are Fierz equivalent to the current–current operators Q_1 and Q_2 . Applying then the $SU(3)$ flavour symmetry to the hadronic matrix elements, we obtain the following result [10, 23, 46]:

$$qe^{i\phi}e^{i\omega} \equiv \frac{-3}{2\lambda^2 R_b} \left[\frac{C_9(\mu) + C_{10}(\mu)}{C_1(\mu) + C_2(\mu)} \right] R_q = (0.68 \pm 0.05)R_q , \quad (39)$$

where the $C_i(\mu)$ are perturbative Wilson coefficients [45]. We observe that the strong phase ω vanishes in the $SU(3)$ limit. The smallness of this phase is actually a model-independent feature, as noted in Ref. [46]. In the remainder of this paper, we use $\omega = 0^\circ$. Making numerical studies, we find that values of ω up to 10° would not have an impact on our analysis. The parameter R_q describes $SU(3)$ -breaking effects. Following Ref. [24], we allow for corrections of 30% by taking $R_q = 1.0 \pm 0.3$. As a theory benchmark scenario, we assume

$$R_q = 1.00 \pm 0.05 , \quad (40)$$

which is based on expected future progress for lattice calculations of the relevant quantities as discussed in more detail in Ref. [24]. Since the CP-violating phase ϕ vanishes in the SM, a sizeable value would be a “smoking gun” signal for the presence of NP.

Following Ref. [16], we parametrize the amplitudes as

$$\begin{aligned} A(B^+ \rightarrow \pi^+ K^0) &= -P' \left[1 + \rho_c e^{i\theta_c} e^{i\gamma} - \frac{1}{3} \hat{a}_C e^{i\Delta_{\hat{C}}} q e^{i\omega} e^{i\phi} r_c e^{i\delta_c} \right] \\ \sqrt{2}A(B^+ \rightarrow \pi^0 K^+) &= P' \left[1 + \rho_c e^{i\theta_c} e^{i\gamma} - \left\{ e^{i\gamma} - \left(1 - \frac{1}{3} \hat{a}_C e^{i\Delta_{\hat{C}}} \right) q e^{i\phi} e^{i\omega} \right\} r_c e^{i\delta_c} \right] \\ A(B_d^0 \rightarrow \pi^- K^+) &= P' \left[1 + \frac{2}{3} a_C e^{i\Delta_C} q e^{i\omega} e^{i\phi} r_c e^{i\delta_c} - r e^{i\delta} e^{i\gamma} \right] \\ \sqrt{2}A(B_d^0 \rightarrow \pi^0 K^0) &= -P' \left[1 - r e^{i\delta} e^{i\gamma} + \left\{ e^{i\gamma} - \left(1 - \frac{2}{3} a_C e^{i\Delta_C} \right) q e^{i\phi} e^{i\omega} \right\} r_c e^{i\delta_c} \right] . \end{aligned} \quad (41)$$

Here we include the colour-suppressed EW penguin topologies through the parameters a_C and \hat{a}_C as well as the CP-conserving phases Δ_C and $\Delta_{\hat{C}}$ for the B_d^0 and B^+ decays, respectively. These quantities, which enter with the EW penguin parameters q and ϕ , are related by the isospin symmetry as

$$a_C = \hat{a}_C, \quad \Delta_C = \Delta_{\hat{C}} , \quad (42)$$

where

$$a_C e^{i\Delta_C} \equiv \frac{\hat{P}'_{EW^C}}{\hat{P}'_{EW} + \hat{P}'_{EW^C}} . \quad (43)$$

The overall normalization of the decay amplitudes in Eq. (41) is given by

$$P' \equiv \frac{\lambda^3 A}{\sqrt{\epsilon}} (\mathcal{P}'_t - \mathcal{P}'_c) , \quad (44)$$

where the primes indicate that we are dealing with $\bar{b} \rightarrow \bar{s}$ transitions. The $B^+ \rightarrow \pi^+ K^0$ amplitude differs from $|P'|$ only through the colour-suppressed EW penguin contributions

and the doubly Cabibbo-suppressed hadronic parameter

$$\rho_c e^{i\theta_c} \equiv \left(\frac{\lambda^2 R_b}{1 - \lambda^2} \right) \left[\frac{\mathcal{P}'_t - \tilde{\mathcal{P}}'_u - \mathcal{A}'}{\mathcal{P}'_t - \mathcal{P}'_c} \right], \quad (45)$$

where $\tilde{\mathcal{P}}'_u$ is a QCD penguin and \mathcal{A}' an annihilation amplitude. This parameter can be determined through the U -spin symmetry of strong interactions from data for the $B^+ \rightarrow K^+ \bar{K}^0$ decay [16, 43]. The most recent analysis gives the following result [40]:

$$\rho_c = 0.03 \pm 0.01, \quad \theta_c = (2.6 \pm 4.6)^\circ, \quad (46)$$

which agrees with the expected order of magnitude of the doubly Cabibbo-suppressed ρ_c . In particular, no anomalously large final-state interaction effects are indicated by the data. It is interesting to note that also the small direct CP asymmetry of $B^+ \rightarrow \pi^+ K^0$ is in agreement with this pattern. The remaining hadronic parameters are given by

$$r_c e^{i\delta_c} \equiv \left(\frac{\lambda^2 R_b}{1 - \lambda^2} \right) \left[\frac{\mathcal{T}' + \mathcal{C}'}{\mathcal{P}'_t - \mathcal{P}'_c} \right] \equiv \frac{\hat{T}' + \hat{C}'}{P'} \quad (47)$$

$$r e^{i\delta} \equiv \left(\frac{\lambda^2 R_b}{1 - \lambda^2} \right) \left[\frac{\mathcal{T}' - (\mathcal{P}'_t - \mathcal{P}'_u)}{\mathcal{P}'_t - \mathcal{P}'_c} \right] \equiv \frac{\hat{T}' - \hat{P}'_{tu}}{P'}, \quad (48)$$

where the normalized amplitudes

$$\hat{T}' = |V_{ub}V_{us}^*| \mathcal{T}' \quad \text{and} \quad \hat{C}' = |V_{ub}V_{us}^*| \mathcal{C}', \quad (49)$$

describe, in analogy to Eq. (14), the colour-allowed and colour-suppressed tree-diagram contributions, respectively.

3.2 Determination of the hadronic parameters

The $B \rightarrow \pi K$ system is related to the $B \rightarrow \pi\pi$ modes through the $SU(3)$ flavour symmetry of strong interactions, which allows us to convert the $B \rightarrow \pi\pi$ parameters determined in Subsection 2.2 into their $B \rightarrow \pi K$ counterparts [16, 17]. As EW penguins play a negligible role in the $B \rightarrow \pi\pi$ system, the resulting hadronic $B \rightarrow \pi K$ parameters are essentially not affected by possible NP contributions to the EW penguin sector.

A complication arises from exchange (E) and penguin-annihilation (PA) topologies, which are present in the $B \rightarrow \pi\pi$ system but do not contribute to the $B \rightarrow \pi K$ modes. These contributions are dynamically suppressed and expected to play a minor role. Using data for $B_s^0 \rightarrow \pi^- \pi^+$ and $B_d^0 \rightarrow K^- K^+$ decays [47], which exclusively emerge from such topologies, and the $SU(3)$ flavour symmetry, the E and PA contributions can be constrained. As discussed in detail in Ref. [40], this results in effects at the few percent level of the overall $B \rightarrow \pi K$ amplitudes. In the future, measurements of CP asymmetries in the $B_s^0 \rightarrow \pi^- \pi^+$ and $B_d^0 \rightarrow K^- K^+$ decays will result in more precise determinations of these effects [40], allowing us to take these corrections into account.

Let us now determine the hadronic $B \rightarrow \pi K$ parameters from $B \rightarrow \pi\pi$ decays. First, we discuss r_c and δ_c with their counterparts in the $B \rightarrow \pi\pi$ system as given in Eq. (9). In the limit of the $SU(3)$ flavour symmetry, we have

$$r_c e^{i\delta_c} = r_c^{\pi\pi} e^{i\delta_c^{\pi\pi}}, \quad (50)$$

which is not affected by factorizable $SU(3)$ -breaking corrections if contributions from the colour-suppressed tree topology are neglected. The $B^+ \rightarrow \pi^+\pi^0$ decay allows us to determine the $|\mathcal{T} + \mathcal{C}|$ amplitude, which can be converted into its $B \rightarrow \pi K$ counterpart using

$$|\mathcal{T}' + \mathcal{C}'| = R_{T+C}|\mathcal{T} + \mathcal{C}|, \quad (51)$$

where R_{T+C} parameterizes $SU(3)$ -breaking effects. We can write this quantity as

$$R_{T+C} = \left| \frac{\mathcal{T}'}{\mathcal{T}} \right| \left| \frac{1 + \kappa'}{1 + \kappa} \right| \quad (52)$$

with

$$\kappa^{(\prime)} \equiv \frac{\mathcal{C}^{(\prime)}}{\mathcal{T}^{(\prime)}}, \quad (53)$$

which is expected to take a value at the 0.3 level. Within the factorization framework, we obtain

$$R_{T+C}|_{\text{fact}} \equiv \left| \frac{\mathcal{T}'}{\mathcal{T}} \right|_{\text{fact}} = \frac{f_K}{f_\pi} = 1.1928 \pm 0.0026, \quad (54)$$

where we have used the numerical value of f_K/f_π given in Ref. [48].

Finally, we may determine $|P'|$ from the $B^+ \rightarrow \pi^+K^0$ branching ratio, yielding the following relation [16]:

$$r_c = \sqrt{2} \left| \frac{V_{us}}{V_{ud}} \right| R_{T+C} \sqrt{r_\rho \left[\frac{\Phi(m_\pi/m_{B^+}, m_{K^0}/m_{B^+})}{\Phi(m_\pi/m_{B^+}, m_{\pi^0}/m_{B^+})} \right] \left[\frac{\mathcal{B}r(B^+ \rightarrow \pi^+\pi^0)}{\mathcal{B}r(B^+ \rightarrow \pi^+K^0)} \right]}, \quad (55)$$

where we take also the small correction from ρ_c through

$$r_\rho = 1 + 2\rho_c \cos \theta_c \cos \gamma + \rho_c^2 \quad (56)$$

with the values in Eq. (46) into account. Using R_{T+C} from Eq. (54) and the most recent values of the CKM matrix elements in Ref. [35] yields

$$r_c = 0.19 \pm 0.01. \quad (57)$$

In Fig. 3a, we compare this determination with $r_c^{\pi\pi}$ and $\delta_c^{\pi\pi}$ in Eq. (37). Here the latter parameters give the red ellipse, whereas the blue circle follows from Eq. (57). In Fig. 3b we zoom in on the red ellipse and show the precision that can be obtained for $r_c^{\pi\pi}$ and $\delta_c^{\pi\pi}$ in the era of Belle II and the LHCb upgrade, using the expected uncertainty for the $B \rightarrow \pi\pi$ observables [4], as well as $\gamma = (70 \pm 1)^\circ$ [4, 5] and $\phi_d = (43.2 \pm 0.6)^\circ$ [44]. We have shifted the ellipse to get agreement with the blue contour, and observe that both constraints have actually similar precision. In order to guide the eye, we have also added the dashed red ellipse which corresponds to the current data.

The impressive agreement between the two determinations in Fig. 3a does not indicate non-factorizable $SU(3)$ -breaking corrections within the current experimental precision. In order to quantify this feature, we reverse Eq. (55) and use it to determine R_{T+C} from the value of r_c in Eq. (37), yielding

$$R_{T+C} = 1.07 \pm 0.23. \quad (58)$$

This value agrees with

$$R_{T+C} = 1.2 \pm 0.2 \quad (59)$$

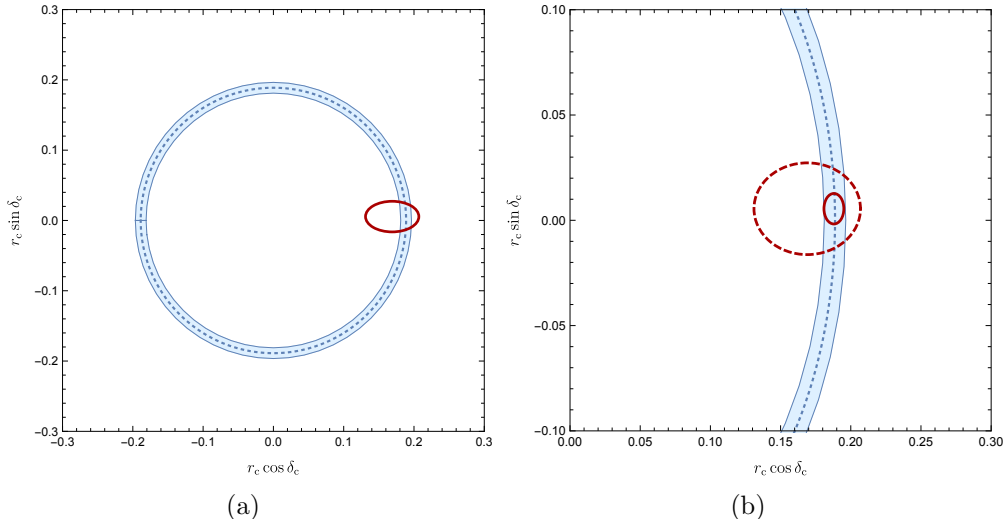


Figure 3: Constraints on r_c and δ_c : (a) the blue circle depicts the 1σ constraints from Eq. (55) with $R_{T+C}|_{\text{fact}}$ while the red ellipse follows from the $B \rightarrow \pi\pi$ data yielding the results in Eq. (37); (b) scenario for the expected future precision as discussed in the text.

given in Ref. [24], where non-factorizable $SU(3)$ -breaking corrections as large as 100% of the factorizable effects in Eq. (54) were considered.

Utilizing non-perturbative QCD sum rule techniques and allowing for non-factorizable effects, the parameter R_{T+C} was calculated in Ref. [49]:

$$R_{T+C} = |(1.21_{-0.014}^{+0.015}) + (0.008_{-0.015}^{+0.013})i| = 1.21 \pm 0.015. \quad (60)$$

Interestingly, a small CP-conserving strong phase arises in this calculation, resembling a picture in analogy to Eq. (37). Moreover, the agreement between Eqs. (54) and (60) indicates that non-factorizable effects have actually a small impact on this parameter.

In the following discussion, R_{T+C} is a key quantity. For the numerical analyses of the current data, we shall use the value in Eq. (59). In view of the discussion in the previous paragraph, the corresponding uncertainty is conservative. As a future benchmark scenario, we follow Ref. [24], and assume

$$R_{T+C} = 1.22 \pm 0.02 \quad (61)$$

as a result from expected progress in lattice QCD calculations.

We include non-factorizable corrections to the relation in Eq. (50) via

$$r_c e^{i\delta_c} = \xi_{SU(3)}^{r_c} r_c^{\pi\pi} e^{i(\Delta_{SU(3)}^{r_c} + \delta_c^{\pi\pi})}, \quad (62)$$

where $\xi_{SU(3)}^{r_c}$ and $\Delta_{SU(3)}^{r_c}$ parametrize the $SU(3)$ -breaking effects. Considering non-factorizable corrections of up to 20% through

$$\xi_{SU(3)}^{r_c} = 1.0 \pm 0.2, \quad \Delta_{SU(3)}^{r_c} = (0 \pm 20)^\circ \quad (63)$$

yields

$$\begin{aligned} r_c &= 0.17 \pm 0.04|_{\text{input}} \pm 0.03|_{SU(3)} = 0.17 \pm 0.05, \\ \delta_c &= (1.9 \pm 7.5|_{\text{input}} \pm 20.0|_{SU(3)})^\circ = (1.9 \pm 21.4)^\circ, \end{aligned} \quad (64)$$

Parameter	Value
γ	$(70 \pm 7)^\circ$
ϕ_d	$(43.2 \pm 1.8)^\circ$
r	0.09 ± 0.03
δ	$(28.6 \pm 21.4)^\circ$
r_c	0.17 ± 0.05
δ_c	$(1.9 \pm 21.4)^\circ$
ρ_c	0.03 ± 0.01
θ_c	$(2.6 \pm 4.6)^\circ$

Table 3: Input and hadronic $B \rightarrow \pi K$ parameters obtained from the current $B \rightarrow \pi\pi$ data, including uncertainties from $SU(3)$ -breaking effects as discussed in Sec. 3.2.

where we give the errors of the individual input parameters and add them in quadrature.

Let us now determine the parameters r and δ which enter the amplitude of the $B_d^0 \rightarrow \pi^- K^+$ channel. They are related to their $B_d^0 \rightarrow \pi^- \pi^+$ counterparts through the $SU(3)$ relation

$$r e^{i\delta} = -\frac{e^{-i\Delta_{SU(3)}^d}}{\xi_{SU(3)}^d} \left[\frac{\epsilon}{d} e^{-i\theta} \right], \quad (65)$$

where $\xi_{SU(3)}^d$ and $\Delta_{SU(3)}^d$ describe non-factorizable $SU(3)$ -breaking corrections. Allowing again for such effects of 20% through

$$\xi_{SU(3)}^d = 1.0 \pm 0.2, \quad \Delta_{SU(3)}^d = (0 \pm 20)^\circ, \quad (66)$$

we find

$$\begin{aligned} r &= 0.09 \pm 0.03|_{\text{input}} \pm 0.02|_{SU(3)} = 0.09 \pm 0.03, \\ \delta &= (28.6 \pm 7.6|_{\text{input}} \pm 20.0|_{SU(3)})^\circ = (28.6 \pm 21.4)^\circ. \end{aligned} \quad (67)$$

These quantities have also been obtained with the help of data for the $B_s^0 \rightarrow \pi^+ K^-$ channel, which is the U -spin partner of the $B_d^0 \rightarrow \pi^- K^+$ decay [40]:

$$\begin{aligned} r &= 0.10 \pm 0.01|_{\text{input}} \pm 0.02|_{SU(3)} = 0.01 \pm 0.02, \\ \delta &= (24.6 \pm 3.3|_{\text{input}} \pm 20.0|_{SU(3)})^\circ = (24.6 \pm 20.3)^\circ. \end{aligned} \quad (68)$$

The impressive agreement between Eqs. (67) and (68) does not indicate any anomalously large $SU(3)$ -breaking effects or contributions from exchange and penguin-annihilation topologies.

3.3 Observables and dynamics

3.3.1 Branching ratios

It is useful to introduce the following ratios of the branching ratios of the four $B \rightarrow \pi K$ modes [10, 46, 50]:

$$R \equiv \left[\frac{\mathcal{B}r(B_d^0 \rightarrow \pi^- K^+)}{\mathcal{B}r(B^+ \rightarrow \pi^+ K^0)} \right] \frac{\tau_{B^+}^{\text{exp}}}{\tau_{B_d^0}^{\text{exp}}} \equiv 0.89 \pm 0.04 , \quad (69)$$

$$R_c \equiv 2 \left[\frac{\mathcal{B}r(B^+ \rightarrow \pi^0 K^+)}{\mathcal{B}r(B^+ \rightarrow \pi^+ K^0)} \right]^{\text{exp}} \equiv 1.09 \pm 0.06 , \quad (70)$$

$$R_n \equiv \frac{1}{2} \left[\frac{\mathcal{B}r(B_d^0 \rightarrow \pi^- K^+)}{\mathcal{B}r(B_d^0 \rightarrow \pi^0 K^0)} \right]^{\text{exp}} \equiv 0.99 \pm 0.06 , \quad (71)$$

where the values are obtained from the current data summarized in Table 2. The ratios R_c and R_n depend on the EW penguin parameters q and ϕ , while R only involves colour-suppressed EW penguins. Using the expressions in Eq. (41), we can express these ratios in terms of the hadronic parameters introduced above.

It is instructive to use the fact that r and r_c are small parameters of $\mathcal{O}(0.1)$, and make expansions in terms of $r_{(c)}$, which yields

$$R_c = 1 - 2 r_c \cos \delta_c (\cos \gamma - q \cos \phi) + \mathcal{O}(r_c^2) , \quad (72)$$

$$R_n = 1 - 2 r_c \cos \delta_c (\cos \gamma - q \cos \phi) + \mathcal{O}(r_c^2) . \quad (73)$$

We note an interesting relation:

$$R_c - R_n = 0 + \mathcal{O}(r_{(c)}^2) = 0.10 \pm 0.08, \quad (74)$$

where the numerical value follows from the experimental results in Eqs. (70) and (71). Consequently, the relation is actually satisfied by the data at the 1σ level.

3.3.2 Colour-suppressed electroweak penguins

In the case of the observable R , we obtain

$$R = 1 - 2 r \cos \delta \cos \gamma + 2 r_c \tilde{a}_C q \cos \phi - 2 \rho_c \cos \theta_c \cos \gamma + \mathcal{O}(r_{(c)}^2, \rho_c^2) , \quad (75)$$

where

$$\tilde{a}_C \equiv a_C \cos(\delta_c + \Delta_C) \quad (76)$$

describes the colour-suppressed EW penguin topologies. The direct CP asymmetry of the $B_d^0 \rightarrow \pi^- K^+$ channel takes the form

$$A_{\text{CP}}^{\pi^- K^+} \equiv \mathcal{A}_{\text{CP}}^{\text{dir}}(B_d^0 \rightarrow \pi^- K^+) = \frac{4}{3} r_c \tilde{a}_S q \sin \phi - 2 r \sin \delta \sin \gamma + \mathcal{O}(r_{(c)}^2) \quad (77)$$

with

$$\tilde{a}_S \equiv a_C \sin(\delta_c + \Delta_C) . \quad (78)$$

The parameter \tilde{a}_S enters also the direct CP asymmetries of the other $B \rightarrow \pi K$ decays. For small phases δ_c (see Eq. (64)) and Δ_C , the sine term results in a strong suppression of

\tilde{a}_S . Having the hadronic parameters in Subsection 3.2 at hand, R and $A_{\text{CP}}^{\pi^- K^+}$ allow the determination of the colour-suppressed EW penguin contributions \tilde{a}_C and \tilde{a}_S . Neglecting sub-leading terms, we find

$$\tilde{a}_S q \sin \phi = \frac{3(A_{\text{CP}}^{\pi^- K^+} + 2r \sin \delta \sin \gamma)}{4r_c}, \quad (79)$$

$$\tilde{a}_C q \cos \phi = \frac{R - 1 + 2r \cos \delta \cos \gamma + 2\rho_c \cos \theta_c \cos \gamma}{2r_c}. \quad (80)$$

Using the parameters in Table 3 gives

$$\tilde{a}_C q \cos \phi = -0.10 \pm 0.15, \quad \tilde{a}_S q \sin \phi = -0.005 \pm 0.274. \quad (81)$$

Assuming the SM value of q in Eq. (39), we obtain

$$\tilde{a}_C|_{\text{SM}} = -0.15 \pm 0.23, \quad (82)$$

which supports the expectation that colour-suppressed EW penguins play a minor role.

3.3.3 Direct CP asymmetries and sum rules

Performing again expansions in the small r_c as well as the tiny ρ_c yields

$$\begin{aligned} A_{\text{CP}}^{\pi^+ K^0} &\equiv A_{\text{CP}}^{\text{dir}}(B^+ \rightarrow \pi^+ K^0) = 2\rho_c \sin \theta_c \sin \gamma - \frac{2}{3}\tilde{a}_S q r_c \sin \phi + \mathcal{O}(r_c^2, \rho_c^2), \\ A_{\text{CP}}^{\pi^0 K^+} &\equiv A_{\text{CP}}^{\text{dir}}(B^+ \rightarrow \pi^0 K^+) = 2\rho_c \sin \theta_c \sin \gamma - 2r_c \sin \delta_c [\sin \gamma - q \sin \phi] \\ &\quad - \frac{2}{3}\tilde{a}_S q r_c \sin \phi + \mathcal{O}(r_c^2, \rho_c^2), \\ A_{\text{CP}}^{\pi^0 K^0} &\equiv A_{\text{CP}}^{\text{dir}}(B_d^0 \rightarrow \pi^0 K^0) = 2r_c \sin \delta_c [\sin \gamma - q \sin \phi] + \frac{4}{3}\tilde{a}_S q r_c \sin \phi \\ &\quad - 2r \sin \delta \sin \gamma + \mathcal{O}(r_{(c)}^2), \end{aligned} \quad (83)$$

which complement the expression in Eq. (77). Interestingly, the contribution from \tilde{a}_S vanishes in the case of $\phi = 0^\circ$, which includes also the SM.

Using the information encoded in the CP-averaged branching ratios, we obtain

$$\begin{aligned} \Delta_{\text{SR}}^{(I)} &= A_{\text{CP}}^{\pi^\pm K^\mp} + A_{\text{CP}}^{\pi^\pm K^0} \frac{\mathcal{B}r(B^+ \rightarrow \pi^+ K^0)}{\mathcal{B}r(B_d^0 \rightarrow \pi^- K^+)} \frac{\tau_{B^0}}{\tau_{B^+}} - A_{\text{CP}}^{\pi^0 K^\pm} \frac{2\mathcal{B}r(B^+ \rightarrow \pi^0 K^+)}{\mathcal{B}r(B_d^0 \rightarrow \pi^- K^+)} \frac{\tau_{B^0}}{\tau_{B^+}} \\ &\quad - A_{\text{CP}}^{\pi^0 K^0} \frac{2\mathcal{B}r(B_d^0 \rightarrow \pi^0 K^0)}{\mathcal{B}r(B_d^0 \rightarrow \pi^- K^+)} = 0 + \mathcal{O}(r_{(c)}^2, \rho_c^2), \end{aligned} \quad (84)$$

which offers an interesting test of the SM. This sum rule was actually pointed out in Refs. [51, 52]. Evaluating the sub-leading terms gives

$$\Delta_{\text{SR}}^{(I)} = 2q r_c \left[\frac{r \sin(\delta_c - \delta) + \rho_c \sin(\delta_c - \theta_c)}{1 - 2r \cos \delta \cos \gamma + r^2} \right] \sin(\gamma - \phi). \quad (85)$$

If we use the hadronic parameters in Subsection 3.2 and the SM values of (q, ϕ) , we obtain the SM prediction

$$\Delta_{\text{SR}}^{(I)}|_{\text{SM}} = -0.009 \pm 0.013. \quad (86)$$

On the other hand, the current data in Table 2 give

$$\Delta_{\text{SR}}^{(\text{I})}|_{\text{exp}} = -0.15 \pm 0.14, \quad (87)$$

which is consistent with zero and the SM prediction within the uncertainties.

In addition, we also study another sum rule [51, 52]:

$$\Delta_{\text{SR}}^{(\text{II})} \equiv A_{\text{CP}}^{\pi^- K^+} + A_{\text{CP}}^{\pi^+ K^0} - A_{\text{CP}}^{\pi^0 K^+} - A_{\text{CP}}^{\pi^0 K^0}, \quad (88)$$

which can be written as

$$\begin{aligned} \Delta_{\text{SR}}^{(\text{II})} = & 2r_c \left\{ \sin(2\delta_c) \left[\sin(2\gamma) - 2q \sin(\gamma + \phi) + q^2 \sin(2\phi) \right] r_c \right. \\ & - \sin(\delta_c + \delta) [\sin(2\gamma) - q \sin(\gamma + \phi)] r \\ & \left. - \sin(\delta_c + \theta_c) [\sin(2\gamma) - q \sin(\gamma + \phi)] \rho_c \right\} + \mathcal{O}(r_c^3, \rho_c^3). \end{aligned} \quad (89)$$

In contrast to Eq. (85), this expression has a q^2 term, thereby showing different sensitivity to a modified EW penguin sector. We find the SM prediction

$$\Delta_{\text{SR}}^{(\text{II})}|_{\text{SM}} = -0.003 \pm 0.028, \quad (90)$$

while the current data give

$$\Delta_{\text{SR}}^{(\text{II})}|_{\text{exp}} = -0.14 \pm 0.13. \quad (91)$$

Comparing Eq. (90) with Eq. (86), we observe that the uncertainty of the second sum rule is larger. This feature is caused by a more pronounced dependence of Eq. (89) on the relevant decay parameters.

The current experimental value of the direct CP asymmetry of the $B_d^0 \rightarrow \pi^0 K^0$ channel suffers from a large uncertainty which actually governs the errors of Eqs. (87) and (91). In fact, the PDG value in Table 2 is an average of BaBar [53] and Belle [54] measurements which show different signs. On the other hand, we may use the sum rules to predict the direct CP violation in $B_d^0 \rightarrow \pi^0 K^0$. Using the cleaner sum rule in Eq. (84) and taking into account higher-order effects from Eq. (85), we find

$$A_{\text{CP}}^{\pi^0 K^0} = -0.14 \pm 0.03. \quad (92)$$

A similar result, with a slightly larger error, follows from Eqs. (88) and (89). The prediction in Eq. (92) lies within the 1σ range of the experimental value in Table 2 but has a much smaller uncertainty. We shall use Eq. (92) as the reference value of $A_{\text{CP}}^{\pi^0 K^0}$.

3.4 Vanishing CP violation in the electroweak penguin sector

An interesting case is given by $\phi = 0^\circ$, which includes the SM but allows also for NP contributions through non-SM values of q . In view of the discussion in Subsection 3.3.2, we neglect contributions from colour-suppressed EW penguin topologies. The observables take then the following forms [16]:

$$R = \frac{1 - 2r \cos \delta \cos \gamma + r^2}{1 + \rho_c^2 + 2\rho_c \cos \gamma \cos \theta_c}, \quad (93)$$

$$R_n = \frac{1}{b} (1 - 2r \cos \delta \cos \gamma + r^2), \quad (94)$$

$$R_c = 1 + \frac{r_c^2 r q - 2\rho_c r_c \cos(\delta_c - \theta_c) (1 - q \cos \gamma) - 2(-q + \cos \gamma) r_c \cos \delta_c}{1 + \rho_c^2 + 2\rho_c \cos \gamma \cos \theta_c}, \quad (95)$$

where $r_q = 1 - 2q \cos \gamma + q^2$ and [16]

$$b \equiv 1 - 2r \cos \delta \cos \gamma + r^2 + 2r_c \cos \delta_c (-q + \cos \gamma) + 2r \cos(\delta - \delta_c) r_c (-1 + q \cos \gamma) + r_c^2 (1 + q^2 - 2q \cos \gamma) . \quad (96)$$

For the CP asymmetries, we find

$$A_{\text{CP}}^{\pi^- K^+} = \frac{-2r \sin \delta \sin \gamma}{1 - 2r \cos \delta \cos \gamma + r^2} , \quad (97)$$

$$A_{\text{CP}}^{\pi^+ K^0} = \frac{2\rho_c \sin \theta_c \sin \gamma}{1 + 2\rho_c \cos \theta_c \cos \gamma + \rho_c^2} , \quad (98)$$

$$A_{\text{CP}}^{\pi^0 K^+} = -\frac{2r_c \sin \delta_c \sin \gamma - 2\rho_c \sin \theta_c \sin \gamma + 2q\rho_c r_c \sin(\delta_c - \theta_c)}{R_c(1 + \rho_c^2 + 2\rho_c \cos \gamma \cos \theta_c)} . \quad (99)$$

In contrast to Ref. [16], we include the tiny parameter ρ_c .

In the case of $B_d^0 \rightarrow \pi^0 K_S$, the final state is a CP-odd eigenstate.¹ Interference between B_d^0 - \bar{B}_d^0 mixing and decays of B_d^0 or \bar{B}_d^0 mesons into the $\pi^0 K_S$ final state gives rise to a mixing-induced CP asymmetry, which satisfies the following general relation [24,55]:

$$S_{\text{CP}}^{\pi^0 K_S} = \sqrt{1 - (A_{\text{CP}}^{\pi^0 K_S})^2} \sin(\phi_d - \phi_{00}) , \quad (100)$$

where

$$A_{\text{CP}}^{\pi^0 K_S} = A_{\text{CP}}^{\pi^0 K^0} = \frac{2 \sin \gamma}{b} \left[-r \sin \delta + r_c (qr \sin(\delta - \delta_c) + \sin \delta_c) \right] \quad (101)$$

is the direct CP asymmetry, ϕ_d denotes the B_d^0 - \bar{B}_d^0 mixing phase given in Eq. (25), and

$$\phi_{00} \equiv \arg(\bar{A}_{00} A_{00}^*) \quad (102)$$

measures the angle between the decay amplitude $A_{00} = A(B_d^0 \rightarrow \pi^0 K^0)$ and its CP conjugate $\bar{A}_{00} = A(\bar{B}_d^0 \rightarrow \pi^0 \bar{K}^0)$. It is useful to introduce

$$(\sin \phi_d)_{\pi^0 K_S} \equiv \sin(\phi_d - \phi_{00}) = \frac{S_{\text{CP}}^{\pi^0 K_S}}{\sqrt{1 - (A_{\text{CP}}^{\pi^0 K_S})^2}} = \left[1 + \frac{1}{2} (A_{\text{CP}}^{\pi^0 K_S})^2 + \dots \right] S_{\text{CP}}^{\pi^0 K_S} . \quad (103)$$

Thanks to the functional dependence of this expression, for the sum rule prediction in Eq. (92), the direct CP asymmetry has only a tiny numerical impact at the 1% level. Consequently, $(\sin \phi_d)_{\pi^0 K_S}$ is fully governed by the mixing-induced CP asymmetry.

The amplitude parametrizations given above yield

$$\tan \phi_{00}|_{\phi=0^\circ} = 2 \left(\frac{Q}{W} \right) \sin \gamma , \quad (104)$$

where

$$\begin{aligned} Q &= r \cos \delta - r_c \cos \delta_c + qr_c^2 - qrr_c \cos(\delta - \delta_c) \\ &\quad - (r_c^2 - 2rr_c \cos(\delta - \delta_c) + r^2) \cos \gamma , \\ W &= 1 - 2(qr_c^2 - r_c \cos \delta_c + r \cos \delta - qrr_c \cos(\delta - \delta_c)) \cos \gamma - 2qr_c \cos(\delta_c) \\ &\quad + (r_c^2 - 2rr_c \cos(\delta - \delta_c) + r^2) \cos(2\gamma) + q^2 r_c^2 . \end{aligned} \quad (105)$$

¹As usual, we neglect tiny CP violation in the neutral kaon system.

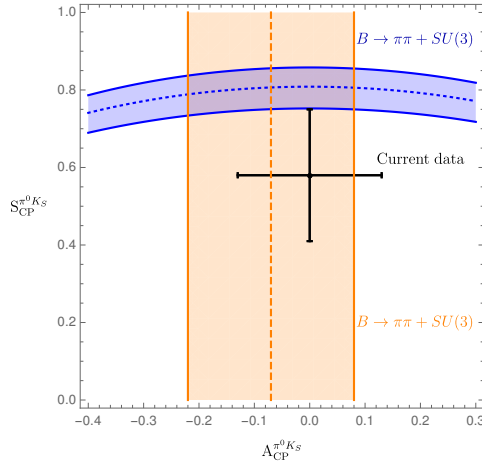


Figure 4: Predictions of the CP-violating $B_d^0 \rightarrow \pi^0 K_S$ observables for the SM values of q and ϕ and the hadronic parameters fixed through the current $B \rightarrow \pi\pi$ data and the $SU(3)$ flavour symmetry.

As the direct CP asymmetry $A_{\text{CP}}^{\pi^0 K_S}$ can be measured, the prediction of the mixing-induced CP asymmetry $S_{\text{CP}}^{\pi^0 K_S}$ requires knowledge of the angle ϕ_{00} , which will play a central role in the remainder of this paper. It is interesting to note that Eq. (104) involves cosine functions of CP-conserving strong phases which are very robust for smallish phases. On the other hand, the direct CP asymmetry in Eq. (101) depends on sine functions which are much more sensitive to the values of the strong phases.

Using the SM value of q in Eq. (39) and the hadronic parameters in Table 3 yields

$$\phi_{00}|_{\text{SM}} = (-10.8 \pm 5.2)^\circ, \quad (106)$$

where the error is dominated by the uncertainty of R_q discussed in Section 3. For $\phi = 0^\circ$, colour-suppressed EW penguins do not contribute to ϕ_{00} at leading order. We have checked that including them has indeed a very minor impact. Moreover, we obtain

$$(\sin \phi_d)_{\pi^0 K_S}|_{\text{SM}} = 0.81 \pm 0.06. \quad (107)$$

The expression in Eq. (101) yields

$$A_{\text{CP}}^{\pi^0 K_S}|_{\text{SM}} = -0.07 \pm 0.15, \quad (108)$$

which allows us to convert $(\sin \phi_d)_{\pi^0 K_S}$ into the mixing-induced CP asymmetry

$$S_{\text{CP}}^{\pi^0 K_S}|_{\text{SM}} = 0.81 \pm 0.07. \quad (109)$$

In Fig. 4, we summarise the current situation in the $A_{\text{CP}}^{\pi^0 K_S}$ - $S_{\text{CP}}^{\pi^0 K_S}$ plane. Here the blue contour corresponds to Eq. (100) with ϕ_{00} given in Eq. (106), whereas the vertical band represents Eq. (108). The black cross shows the current data. We observe that the mixing-induced CP asymmetry exhibits a deviation from the measured value at the 1σ level. The value of $A_{\text{CP}}^{\pi^0 K_S}$ is in full agreement with the data and the sum rule prediction in Eq. (92) having a much smaller uncertainty.

In Table 4, we summarize the SM predictions and experimental data for the various $B \rightarrow \pi K$ observables. The errors are dominated by the currently large uncertainty of the

Observable	SM Prediction	Experiment
R	0.93 ± 0.03	0.89 ± 0.04
R_n	1.13 ± 0.10	0.99 ± 0.06
R_c	1.11 ± 0.08	1.09 ± 0.06
$A_{\text{CP}}^{\pi^\pm K^\mp}$	-0.085 ± 0.064	-0.082 ± 0.006
$A_{\text{CP}}^{\pi^\pm K^0}$	0.003 ± 0.005	-0.017 ± 0.016
$A_{\text{CP}}^{\pi^0 K^\pm}$	-0.007 ± 0.11	0.037 ± 0.021
$A_{\text{CP}}^{\pi^0 K_S}$	-0.07 ± 0.15	0.00 ± 0.13
$S_{\text{CP}}^{\pi^0 K_S}$	0.81 ± 0.07	0.58 ± 0.17
$\mathcal{B}r(B_d^0 \rightarrow \pi^- K^+) \times 10^6$	20.6 ± 0.7	19.6 ± 0.5
$\mathcal{B}r(B^+ \rightarrow \pi^+ K^0) \times 10^6$	Normalization	23.7 ± 0.8
$\mathcal{B}r(B^+ \rightarrow \pi^0 K^+) \times 10^6$	13.1 ± 1.0	12.9 ± 0.5
$\mathcal{B}r(B_d^0 \rightarrow \pi^0 K^0) \times 10^6$	9.1 ± 0.9	9.9 ± 0.5

Table 4: SM predictions of the $B \rightarrow \pi K$ observables and comparison with the current experimental data.

$SU(3)$ -breaking parameter R_q . For the branching ratios, we use the measured branching ratio of $B^+ \rightarrow \pi^+ K^0$ to fix the normalization $|P'|$. We observe that all predictions are well within the current experimental measurements. The excellent agreement of R and $A_{\text{CP}}^{\pi^- K^+}$ with the measurements reflects the smallness of the colour-suppressed EW penguin contributions found in Subsection 3.3.2, where these observables were used to determine the colour-suppressed EW penguin parameters. The largest deviation arises in the ratio R_n , where there is a tension of a bit more than 1σ significance.

4 Correlations between CP asymmetries of $B_d^0 \rightarrow \pi^0 K_S$

4.1 Preliminaries

The mixing-induced CP asymmetry of the $B_d^0 \rightarrow \pi^0 K_S$ channel is a particularly interesting probe for testing the SM. In the previous section, we have used hadronic parameters which were determined from $B \rightarrow \pi\pi$ data by means of the $SU(3)$ flavour symmetry, resulting in the picture shown in Fig. 4. Interestingly, we can obtain a much more precise correlation in the $A_{\text{CP}}^{\pi^0 K_S} - S_{\text{CP}}^{\pi^0 K_S}$ plane [24], as we will discuss in this section.

The starting point is given by the following isospin relations [6, 7]:

$$\sqrt{2}A(B_d^0 \rightarrow \pi^0 K^0) + A(B^0 \rightarrow \pi^- K^+) = -(\hat{T}' + \hat{C}')e^{i\gamma} + \left(\hat{P}'_{EW} + \hat{P}'_{EW}^C\right) \equiv 3A_{3/2}, \quad (110)$$

$$\sqrt{2}A(\bar{B}_d^0 \rightarrow \pi^0 \bar{K}^0) + A(\bar{B}^0 \rightarrow \pi^+ K^-) = 3\bar{A}_{3/2}, \quad (111)$$

where the isospin $I = 3/2$ amplitude $A_{3/2}$ and its CP-conjugate $\bar{A}_{3/2}$ are given by

$$3A_{3/2} \equiv 3|A_{3/2}|e^{i\phi_{3/2}} = -\left[\hat{T}' + \hat{C}'\right] (e^{i\gamma} - qe^{+i\phi}), \quad (112)$$

$$3\bar{A}_{3/2} \equiv 3|\bar{A}_{3/2}|e^{i\bar{\phi}_{3/2}} = -\left[\hat{T}' + \hat{C}'\right] (e^{-i\gamma} - qe^{-i\phi}). \quad (113)$$

Here we have used $\omega = 0$ and observe the relation

$$\bar{\phi}_{3/2} = -\phi_{3/2}. \quad (114)$$

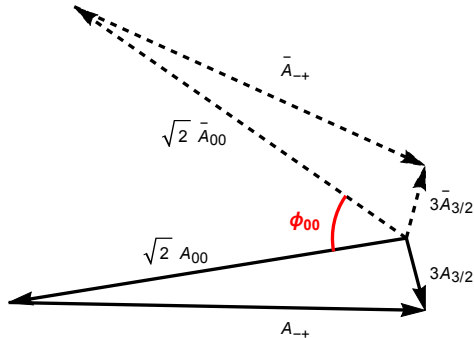


Figure 5: Illustration of the amplitude triangles following from the isospin relations in Eqs. (110) and (111). The solid triangle corresponds to the $B_d^0 \rightarrow \pi^0 K^0$, $B_d^0 \rightarrow \pi^- K^+$ decays while the dashed one represents the CP-conjugate processes.

The absolute value of the amplitude $\hat{T}' + \hat{C}'$ can be fixed through the measured branching ratio of the $B^\pm \rightarrow \pi^0 \pi^\pm$ decay with the help of the $SU(3)$ flavour symmetry [8]:

$$|\hat{T}' + \hat{C}'| = R_{T+C} \left| \frac{V_{us}}{V_{ud}} \right| \sqrt{2} |A(B^+ \rightarrow \pi^+ \pi^0)|. \quad (115)$$

As was pointed out in Ref. [24], using measured CP-averaged branching ratios and direct CP asymmetries, the amplitude relations in Eqs. (110–115) allow us to determine the angle ϕ_{00} for given values of the EW penguin parameters q and ϕ , in particular also for the SM case as described by Eq. (39). Having ϕ_{00} at hand, the expression in Eq. (100) allows us to calculate a contour in the $A_{\text{CP}}^{\pi^0 K_S} - S_{\text{CP}}^{\pi^0 K_S}$ plane. The corresponding correlation relies only on the clean isospin relations in Eqs. (110) and (111) and the $SU(3)$ input given by R_{T+C} in Eq. (115), which is a very robust parameter as discussed in Section 3.2.

It is instructive to have a closer look at the corresponding analysis. The isospin relation in Eq. (110) can be represented by an amplitude triangle in the complex plane as depicted in Fig. 5. For given EW penguin parameters q and ϕ , such as in the SM which we consider in the following discussion, the amplitudes $A_{3/2}$ and $\bar{A}_{3/2}$ are fixed. Using the direct asymmetries $A_{\text{CP}}^{\pi^0 K_S}$ and $A_{\text{CP}}^{\pi^- K^+}$ taking the forms

$$A_{\text{CP}}^{\pi^0 K_S} = \frac{|\bar{A}_{00}|^2 - |A_{00}|^2}{|\bar{A}_{00}|^2 + |A_{00}|^2}, \quad A_{\text{CP}}^{\pi^- K^+} = \frac{|\bar{A}_{-+}|^2 - |A_{-+}|^2}{|\bar{A}_{-+}|^2 + |A_{-+}|^2} \quad (116)$$

with $|A_{-+}| \equiv |A(B_d^0 \rightarrow \pi^- K^+)|$ and $|\bar{A}_{-+}| \equiv |A(\bar{B}_d^0 \rightarrow \pi^+ K^-)|$, and the CP-averaged branching ratios allows the determination of the absolute values of the individual amplitudes. Finally, we determine ϕ_{00} and subsequently $S_{\text{CP}}^{\pi^0 K_S}$ using Eq. (100). Since the triangles can be flipped around the $A_{3/2}$ and $\bar{A}_{3/2}$ axes, we obtain a four-fold ambiguity for ϕ_{00} and correspondingly for $S_{\text{CP}}^{\pi^0 K_S}$.

Let us illustrate this method by taking $A_{\text{CP}}^{\pi^0 K_S}$ from the sum rule in Eq. (92) and central values of the measured observables. The four orientations of the resulting triangles are shown in Fig. 6, and correspond to the angles ϕ_{00} and mixing-induced CP asymmetries $S_{\text{CP}}^{\pi^0 K_S}$ given in Table 5. The triangles are drawn in arbitrary units, since only the shape of the triangles is important for the determination of ϕ_{00} .

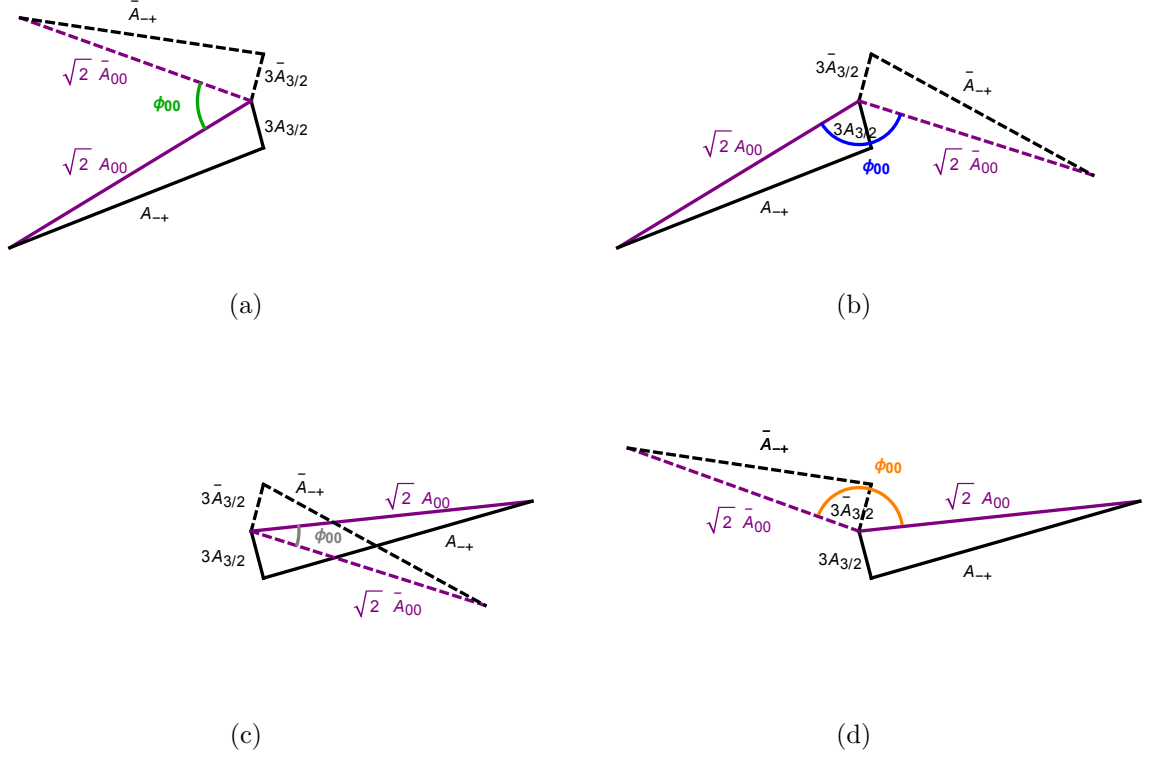


Figure 6: The four orientations of the amplitude triangles for current data and $A_{\text{CP}}^{\pi^0 K_S}$ in Eq. (92). Varying $A_{\text{CP}}^{\pi^0 K_S}$, the triangle configurations correspond to the contours in the $A_{\text{CP}}^{\pi^0 K_S} - S_{\text{CP}}^{\pi^0 K_S}$ plane shown in Fig. 7 with the same colour.

If we now vary the direct CP asymmetry of $B_d^0 \rightarrow \pi^0 K_S$, we obtain a correlation between $S_{\text{CP}}^{\pi^0 K_S}$ and $A_{\text{CP}}^{\pi^0 K_S}$ [16, 24]. This results in the four contours in the $A_{\text{CP}}^{\pi^0 K_S} - S_{\text{CP}}^{\pi^0 K_S}$ plane shown in Figs. 7a and 7b, where we have also taken the experimental errors and the uncertainties of R_{T+C} and R_q into account. The four contours correspond to the configurations in Fig. 5 where ϕ_{00} is labelled with the same colour. We have also included the current experimental data point for the CP asymmetries from Table 2, and the vertical band refers to the sum rule value of $A_{\text{CP}}^{\pi^0 K_S}$ in Eq. (92). In addition, the narrow bands illustrate a future scenario including only the expected theory uncertainties for R_q and R_{T+C} in Eqs. (40) and Eq. (61), respectively.

ϕ_{00}	$S_{\text{CP}}^{\pi^0 K_S}$	ϕ_{00}	$S_{\text{CP}}^{\pi^0 K_S}$
-49.8°	0.989	-22.9°	0.903
128.9°	-0.988	145.5°	-0.967

Table 5: The angles ϕ_{00} and the corresponding mixing-induced CP asymmetries $S_{\text{CP}}^{\pi^0 K_S}$ following from the triangle construction for current data using $A_{\text{CP}}^{\pi^0 K_S}$ in Eq. (92).

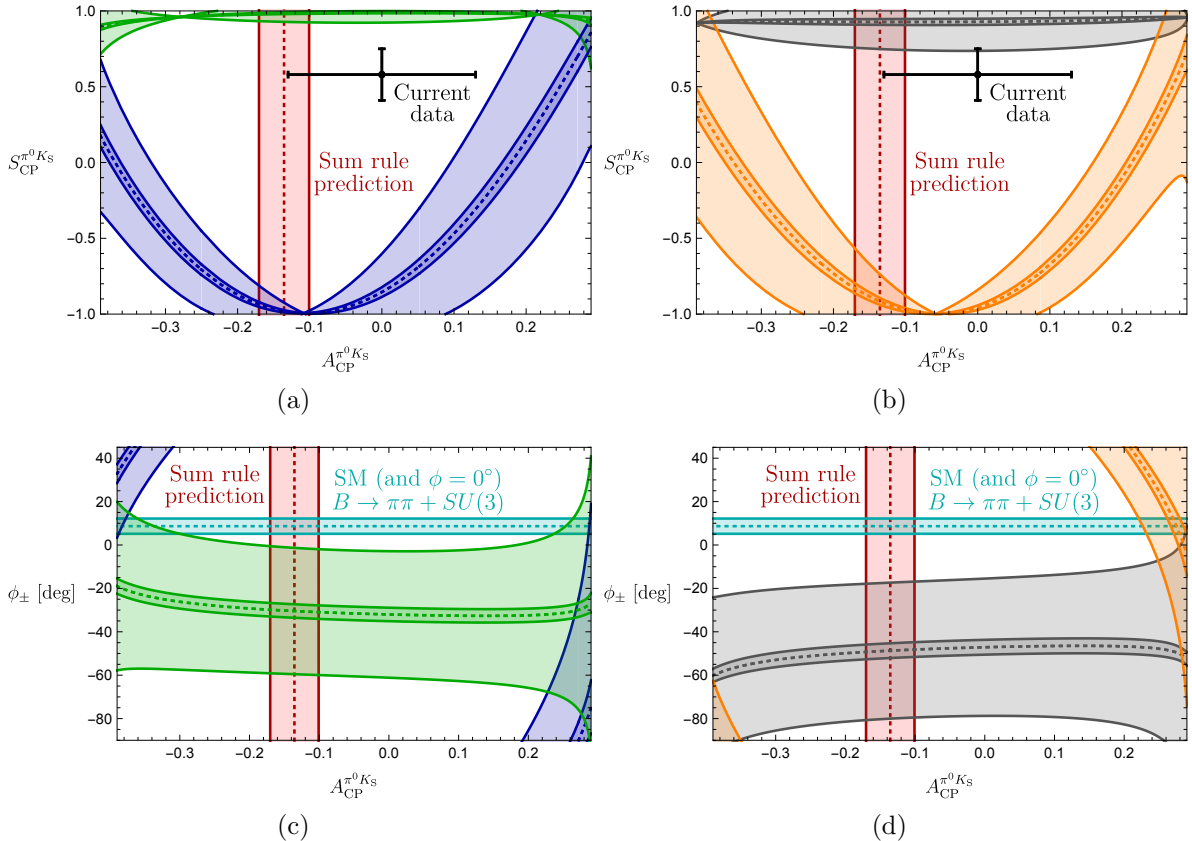


Figure 7: (a, b) Correlations between the CP asymmetries of $B_d^0 \rightarrow \pi^0 K_S$ following from the isospin triangles illustrated in Fig. 6. The vertical band (red) gives the sum rule prediction in Eq. (92). (c, d) For each of the triangle configurations we show the associated angle ϕ_{\pm} . The horizontal band (blue) gives the current SM constraint in Eq. (121). The narrow bands correspond to a future scenario discussed in the text.

4.2 Discrete ambiguities

The four-fold ambiguity arising from the different orientations of the amplitude triangles can be distinguished through the strong phase δ_c [24]. The values of δ_c corresponding to different points on the four contours in Figs. 7a and 7b can be found by parametrizing $A_{\text{CP}}^{\pi^0 K_S}$ and $S_{\text{CP}}^{\pi^0 K_S}$ in terms of the hadronic parameters using Eqs. (100) and (101). Employing now only the neutral $B \rightarrow \pi K$ observables, the hadronic parameters r , δ and r_c can be expressed in terms of the strong phase δ_c using the ratio R_n and $A_{\text{CP}}^{\pi^- K^+}$. In addition, we use $\mathcal{B}r(B_d^0 \rightarrow \pi^- K^+)$ to fix the normalization $|P'|$ which then enters r_c via

$$r_c = \sqrt{2} \left| \frac{V_{us}}{V_{ud}} \right| R_{T+C} \sqrt{\frac{\mathcal{B}r(B^+ \rightarrow \pi^0 \pi^+)}{\mathcal{B}r(B_d^0 \rightarrow \pi^- K^+)} \frac{\tau_{B_d^0}}{\tau_{B^+}} \sqrt{1 + r^2 - 2r \cos \delta \cos \gamma}}, \quad (117)$$

where we used again the $SU(3)$ flavour symmetry.

Finally, we find that the contours in Fig. 7a correspond to $|\delta_c| < 90^\circ$, while those in Fig. 7b give $|\delta_c| > 90^\circ$. Using the range of δ_c in Eq. (64), only the contours in Fig. 7a are allowed. Going one step further, we can also consider the associated value of r_c for the contours in Fig. 7a. We find that the lower contour implies very large values of r_c that are excluded from Eq. (64), thereby leaving only the upper contour in Fig. 7a. In

comparison with Ref. [24], we already obtain a much sharper picture due to the improved value of γ in Eq. (12), which pushes $S_{\text{CP}}^{\pi^0 K^s}$ close to its maximal value of 1. We observe a discrepancy between the data and the triangle constraint at the 2.5σ level.

As a new element, we employ the angle

$$\phi_{\pm} = \text{Arg} [\bar{A}_{-+} A_{-+}^*] \quad (118)$$

between the decay amplitudes $A_{-+} \equiv A(B_d^0 \rightarrow \pi^- K^+)$ and $\bar{A}_{-+} \equiv A(\bar{B}_d^0 \rightarrow \pi^+ K^-)$ [25]. In Figs. 7c and 7d, we give ϕ_{\pm} for each of the four triangle configurations. The narrow band depicts the future theory scenario as discussed above.

In the SM, we may actually calculate ϕ_{\pm} from the hadronic parameters in Eq. (67). For $\phi = 0^\circ$, we obtain

$$\tan \phi_{\pm}|_{\phi=0^\circ} = \frac{-r^2 \sin 2\gamma + r \sin(\gamma - \delta) + r \sin(\gamma + \delta) + C_{\pm}}{1 + r^2 \cos 2\gamma - r \cos(\gamma - \delta) - r \cos(\gamma + \delta) + B_{\pm}}, \quad (119)$$

where

$$\begin{aligned} B_{\pm} &= \frac{4}{3} q r_c [\tilde{a}_C - r \cos \gamma (\tilde{a}_C \cos \delta + \tilde{a}_S \sin \delta) + \frac{1}{3} q r_c (\tilde{a}_C^2 + \tilde{a}_S^2)] \\ C_{\pm} &= \frac{4}{3} q r r_c \sin \gamma (\tilde{a}_C \cos \delta + \tilde{a}_S \sin \delta). \end{aligned} \quad (120)$$

The B_{\pm} and C_{\pm} actually give tiny numerical contributions, and we find

$$\phi_{\pm} = 2r \cos \delta \sin \gamma + \mathcal{O}(r_{(e)}^2) = (8.7 \pm 3.5)^\circ, \quad (121)$$

where we have used the values of r, δ and γ in Table 3 to obtain the numerical result. We have added this SM constraint to Fig. 7 and note that two of the contours in Figs. 7a and 7b are excluded by the new constraint ϕ_{\pm} . This can also be seen in the illustration of the triangles in Fig. 6. In addition, the grey contour in Fig. 7d is in tension with the constraint on ϕ_{\pm} . However, this specific configuration was already excluded because it implies $|\delta_c| > 90^\circ$. We therefore focus on the (green) upper contour in Fig. 7a. However, for this configuration, we observe a tension with the SM prediction for ϕ_{\pm} which is currently at the 1σ level but may become much more pronounced as illustrated by the narrow band referring to a future scenario.

4.3 How to resolve the $B \rightarrow \pi K$ puzzle?

In Fig. 8, we summarize the intriguing picture following from the isospin triangles, showing only the contour remaining once the constraints from Section 4.2 have been applied. In comparison with Fig. 4, we obtain a much cleaner picture, requiring only $SU(3)$ input from R_{T+C} and R_q , which are very robust as discussed in Section 3. On the other hand, Fig. 4 relies on the $SU(3)$ flavour symmetry for the determination of the hadronic $B \rightarrow \pi K$ parameters from their $B \rightarrow \pi\pi$ counterparts.

Obviously, the observed tension with the SM in Fig. 8 could be resolved by a change of the data. However, it is far from trivial to fulfil all constraints simultaneously and an interesting question to explore how the data would have to change in order to get agreement with the SM. In view of the large experimental uncertainty of the $B_d^0 \rightarrow \pi^0 K^0$ branching ratio, this quantity is a prime candidate. In fact, we find that lowering the

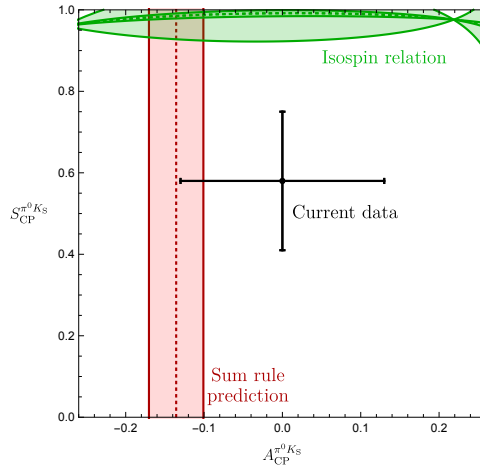


Figure 8: Illustration of the $B \rightarrow \pi K$ puzzle: the upper green band follows from the isospin analysis while the vertical band shows the sum rule prediction in Eq. (92).

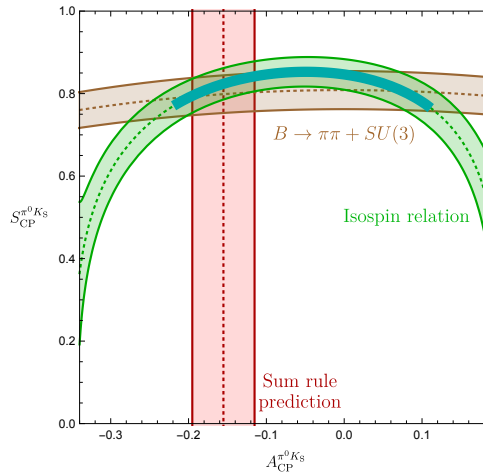


Figure 9: Reducing $\mathcal{B}r(B_d^0 \rightarrow \pi^0 K^0)$ by 2.5σ gives a picture consistent with the SM, where the dark part agrees perfectly with the ϕ_{\pm} constraint in Eq. (121).

central value of $\mathcal{B}r(B_d^0 \rightarrow \pi^0 K^0)$ by about 2.5σ gives a picture which is fully consistent with the SM, provided also the central value of the mixing-induced CP asymmetry of $B_d^0 \rightarrow \pi^0 K^0$ would move up by about 1σ . We illustrate the corresponding situation in Fig. 9, where the part of the contour that is in agreement with the constraint on ϕ_{\pm} in Eq. (118) is highlighted in cyan. In addition, the triangle determination agrees also with the brown SM band following from Eq. (100) with ϕ_{00} in Eq. (104) and the sum rule prediction in Eq. (92).

On the other hand, the puzzling situation may also be a signal of NP effects in the EW penguin sector, thereby affecting the values of q and ϕ . A particularly exciting aspect is the sensitivity to new sources of CP violation.

5 Extracting the electroweak penguin parameters

5.1 Preliminaries

In the previous section, we have used the isospin relations in Eqs. (110) and (111) to calculate a correlation between the direct and mixing-induced CP asymmetries of the $B_d^0 \rightarrow \pi^0 K_S$ channel, resulting in an intriguing picture for the current experimental data that may be an indication of a modified EW penguin sector. In view of this result and to test the corresponding SM sector, it would be very interesting to determine the EW penguin parameters q and ϕ from experimental data and to compare the corresponding results with the SM prediction (see Eq. (39)). The parameter R_q is then only needed for the SM prediction of q while the CP-violating phase ϕ , which vanishes in the SM, may give a “smoking-gun” signal of new sources of CP violation.

In order to achieve this goal, we apply again the isospin relations in Eqs. (110) and (111) for the neutral $B \rightarrow \pi K$ decays. These relations have also counterparts in the system of the charged $B \rightarrow \pi K$ decays, where the $B^+ \rightarrow \pi^0 K^+$ mode receives significant contributions from colour-allowed EW penguin topologies. We have

$$\sqrt{2}A(B^+ \rightarrow \pi^0 K^+) + A(B^+ \rightarrow \pi^+ K^0) = 3A_{3/2} \equiv 3|A_{3/2}|e^{i\phi_{3/2}} \quad (122)$$

$$\sqrt{2}A(B^- \rightarrow \pi^0 K^-) + A(B^- \rightarrow \pi^- \bar{K}^0) = 3\bar{A}_{3/2} \equiv 3|\bar{A}_{3/2}|e^{i\bar{\phi}_{3/2}}, \quad (123)$$

where the isospin amplitude $A_{3/2}$ and its CP-conjugate $\bar{A}_{3/2}$ are given in Eqs. (112) and (113), respectively.

In view of the large experimental uncertainties of the CP-violating observables of the $B_d^0 \rightarrow \pi^0 K_S$ channel, let us focus on the charged $B \rightarrow \pi K$ decays. Using the corresponding CP-averaged branching ratios and direct CP asymmetries, the isospin relations in Eqs. (122) and (123) can be represented as amplitude triangles in the complex plane for a given value of $|A_{3/2}| = |\bar{A}_{3/2}|$. The relative orientation of the triangles is fixed through the tiny angle

$$\phi_c \equiv \text{Arg} [\bar{A}_{+0} A_{+0}^*] = \mathcal{O}(1^\circ) \quad (124)$$

between $A_{+0} \equiv A(B^+ \rightarrow \pi^+ K^0)$ and $\bar{A}_{+0} \equiv A(B^- \rightarrow \pi^- \bar{K}^0)$. Employing Eq. (41) for the $B^+ \rightarrow \pi^+ K^0$ amplitude and neglecting the colour-suppressed EW penguin contributions (see Subsection 3.3.2), we obtain

$$\tan \phi_c = \frac{-\rho_c^2 \sin 2\gamma - \rho_c \sin(\gamma - \theta_c) - \rho_c \sin(\gamma + \theta_c)}{1 + \rho_c^2 \cos 2\gamma + \rho_c \cos(\gamma - \theta_c) + \rho_c \cos(\gamma + \theta_c)}. \quad (125)$$

Using then the values of the corresponding parameters in Table 3 yields

$$\phi_c = (-3.2 \pm 1.1)^\circ. \quad (126)$$

In Fig. 11a, we illustrate the charged $B \rightarrow \pi K$ isospin triangles for the central values of the current data, assuming the SM values of the EW penguin parameters. The triangle construction allows us to determine the difference

$$\Delta\phi_{3/2} \equiv \phi_{3/2} - \bar{\phi}_{3/2} \quad (127)$$

between the phases $\phi_{3/2}$ and $\bar{\phi}_{3/2}$ of the amplitudes $A_{3/2}$ and $\bar{A}_{3/2}$, respectively, which is given by $\Delta\phi_{3/2} = 2\phi_{3/2}$ as can be seen in Eq. (114). Introducing

$$N \equiv 3|A_{3/2}|/|\hat{T}' + \hat{C}'|, \quad (128)$$

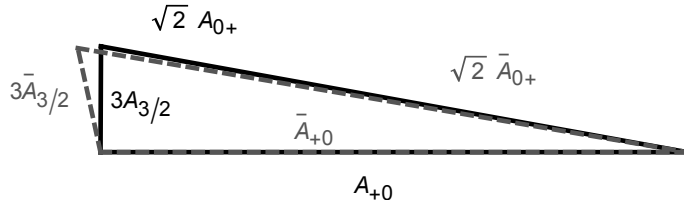


Figure 10: Illustration of the isospin triangles for the charged $B \rightarrow \pi K$ decays with $|A_{3/2}| = |\bar{A}_{3/2}|$.

we obtain

$$q = \sqrt{N^2 - 2c \cos \gamma - 2s \sin \gamma + 1} \quad (129)$$

and

$$\tan \phi = \frac{\sin \gamma - s}{\cos \gamma - c}, \quad q \sin \phi = \sin \gamma - s \quad (130)$$

with

$$c \equiv \pm N \cos(\Delta\phi_{3/2}/2), \quad s \equiv \pm N \sin(\Delta\phi_{3/2}/2), \quad (131)$$

allowing us to calculate contours in the ϕ - q plane. In order to convert the given value of $|A_{3/2}| = |\bar{A}_{3/2}|$ into the parameter N , we use again the $SU(3)$ relation in Eq. (115).

For the current charged $B \rightarrow \pi K$ decay data, we arrive at the contours shown in Fig. 11a. As was the case in Section 4, we have a four-fold ambiguity for $\Delta\phi_{3/2}$ since the triangles can be flipped around the $A_{3/2}$ and $\bar{A}_{3/2}$ axes. This is represented by the four different colours for the contours in Fig. 10. Moreover, for every value of $\Delta\phi_{3/2}$, there are two contours in the ϕ - q plane due to solving a quadratic equation, giving two contours of every colour and eight contours in total. We find discontinuities of the contours around $q \sim 1$, $\phi \sim 70^\circ$, because $|A_{3/2}|$ cannot become arbitrarily small as then the amplitudes in Eq. (122) cannot form triangles anymore.

As in the neutral case, we can eliminate some contours by considering the angle

$$\phi_{0+} = \text{Arg} [\bar{A}_{0+} A_{0+}^*], \quad (132)$$

where $A_{0+} \equiv A(B^+ \rightarrow \pi^0 K^+)$ and $\bar{A}_{0+} \equiv A(B^- \rightarrow \pi^0 K^-)$. We may now compare ϕ_{0+} as obtained from the triangle construction with its theoretical prediction:

$$\tan \phi_{0+} = 2r_c \left[\cos \delta_c \sin \gamma - \left(\cos \delta_c - \frac{1}{3} \tilde{a}_C \right) q \sin \phi \right] + \mathcal{O}(r_{(c)}^2, \rho_c), \quad (133)$$

where the colour-suppressed EW penguin parameter \tilde{a}_C was defined in Eq. (76). These effects can be included using the ratio R via Eq. (80). Contrary to the SM case discussed above, now the theoretically allowed ϕ_{0+} depends on q and ϕ . At the same time, the ϕ_{0+} obtained from the triangle construction also depends on ϕ . In Fig. 11, we show this angle for each of the eight branches of the triangle determinations in the same colour. In addition, in grey we show the theoretically allowed values of ϕ_{0+} as a function of ϕ , using the exact expression but neglecting colour-suppressed EW penguin contributions. For this theoretical prediction, we use the q as a function of ϕ from the associated triangle

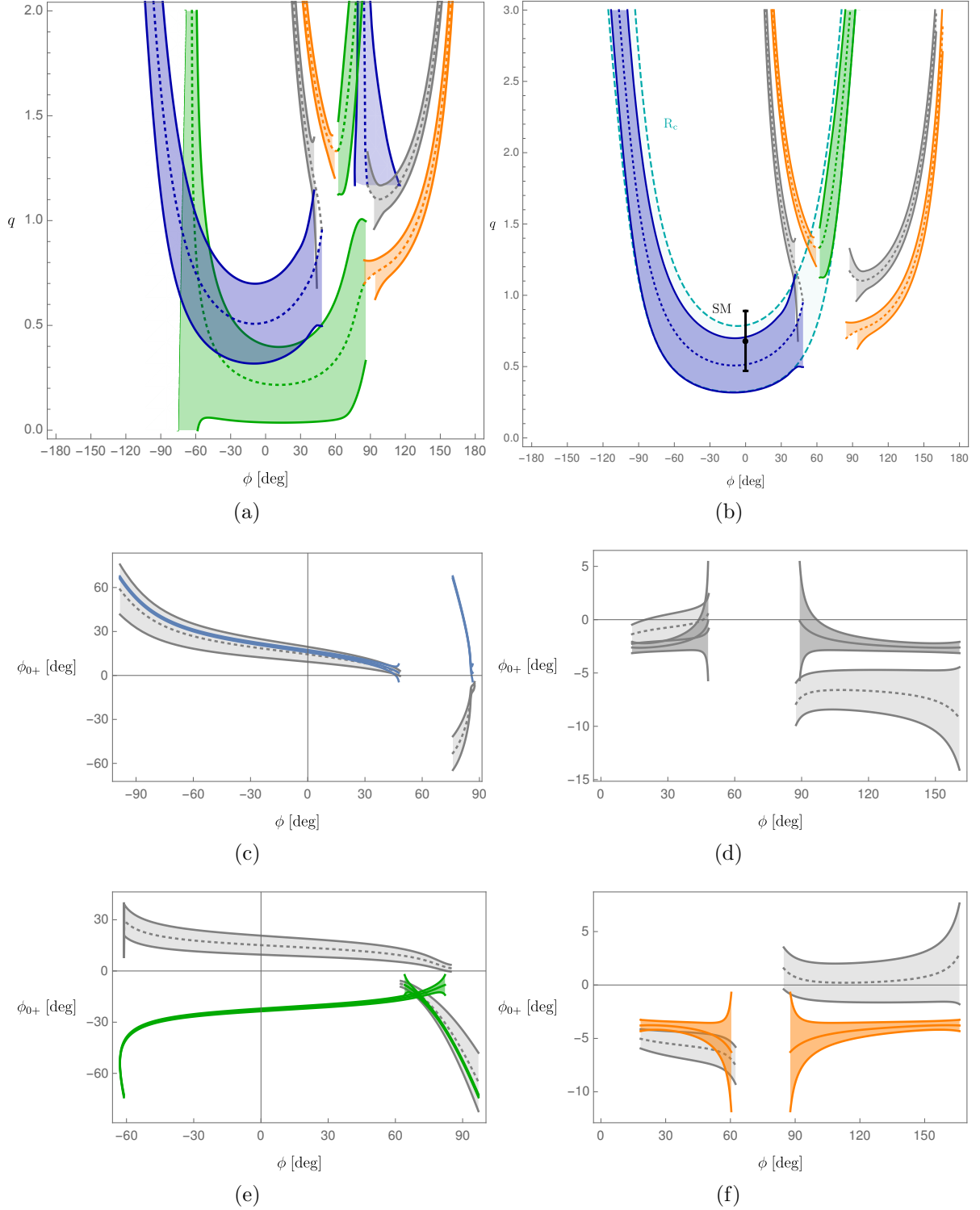


Figure 11: (a) Contours in the ϕ - q plane for the current data for the charged $B \rightarrow \pi K$ decays. (b) Contours remaining after imposing the constraints discussed in the text. (c-f) Theory constraints (grey) combined with the ϕ_{0+} constraint following from the triangle constructions in the same colours.

contour. This implies that each of the eight triangle contours has a different theoretical prediction for ϕ_{0+} as function of ϕ . We observe that one of the contours in Fig. 11c

and one in Fig. 11e is clearly excluded by the theoretical constraint on ϕ_{0+} . We have removed those curves in Fig. 11b.

It is interesting to have a closer look at the ratio R_c of the CP-averaged branching ratios of the charged $B \rightarrow \pi K$ decays introduced in Eq. (72). It allows us to derive the following exact expression:

$$q = \frac{-B_{R_c} \pm \sqrt{B_{R_c}^2 - 4A_{R_c}C_{R_c}}}{2A_{R_c}}, \quad (134)$$

where

$$A_{R_c} \equiv r_c^2, \quad (135)$$

$$B_{R_c} \equiv 2r_c [\cos \delta_c \cos \phi - (r_c - \rho_c \cos(\theta_c - \delta_c)) \cos(\gamma - \phi)], \quad (136)$$

$$C_{R_c} \equiv [1 + 2\rho_c \cos \theta_c \cos \gamma + \rho_c^2] [1 - R_c] - 2\rho_c r_c \cos(\theta_c - \delta_c) - 2r_c \cos \delta_c \cos \gamma + r_c^2. \quad (137)$$

Using the information for r_c and δ_c in Eq. (64) and including also the tiny ρ_c parameter as given in Eq. (46), the measured value of R_c can be converted into yet another contour in the ϕ - q plane. In contrast to the analysis using the isospin relations, we require now also the strong phase δ_c . In Fig. 11b, we have added the resulting contour, which is in excellent agreement with two branches of the isospin triangle construction. This curve is actually also consistent with the SM value of q and ϕ .

We note that the allowed parameter space for q and ϕ following from the current data of the charged $B \rightarrow \pi K$ system is significantly reduced in comparison with the situation discussed in Ref. [24]. Moreover, we have presented a transparent way to calculate the contours in the ϕ - q plane and do not have to make a fit to the data. The constraints on q and ϕ have actually a highly non-trivial structure that follows from the isospin relation and can be understood in an analytic way. The only additional $SU(3)$ input is the quantity R_{T+C} discussed in Section 3.2, which is required for the conversion of $|A_{3/2}|$ into the parameter N .

In Fig. 12a, we discuss the uncertainties of the various input parameters, focusing on the contour in the ϕ - q plane in Fig. 11b that is in agreement with the R_c constraint. When adding the individual errors in quadrature, we obtain the uncertainty band in Fig. 11b. In Fig. 12b, we illustrate the error budget as a pie chart. We observe that γ and the branching ratios play the major roles, while R_{T+C} has a slightly smaller impact on the error budget.

In analogy to the discussion of the charged $B \rightarrow \pi K$ system given above, we may also use the neutral $B \rightarrow \pi K$ decays and their isospin amplitude relations to determine contours in the ϕ - q plane. The key difference is that the measurement of the mixing-induced CP asymmetry of $B_d^0 \rightarrow \pi^0 K_S$ allows us to determine the angle ϕ_{00} in a clean way through Eq. (103), thereby fixing the relative orientation of the neutral $B \rightarrow \pi K$ isospin triangle and its CP conjugate. In contrast to using ϕ_c in Eq. (124) for the charged $B \rightarrow \pi K$ decays, this determination is theoretically clean (although also ϕ_c is only affected by a small theoretical uncertainty). The charged and neutral $B \rightarrow \pi K$ decays should result in constraints in the ϕ - q plane that are consistent with each other.

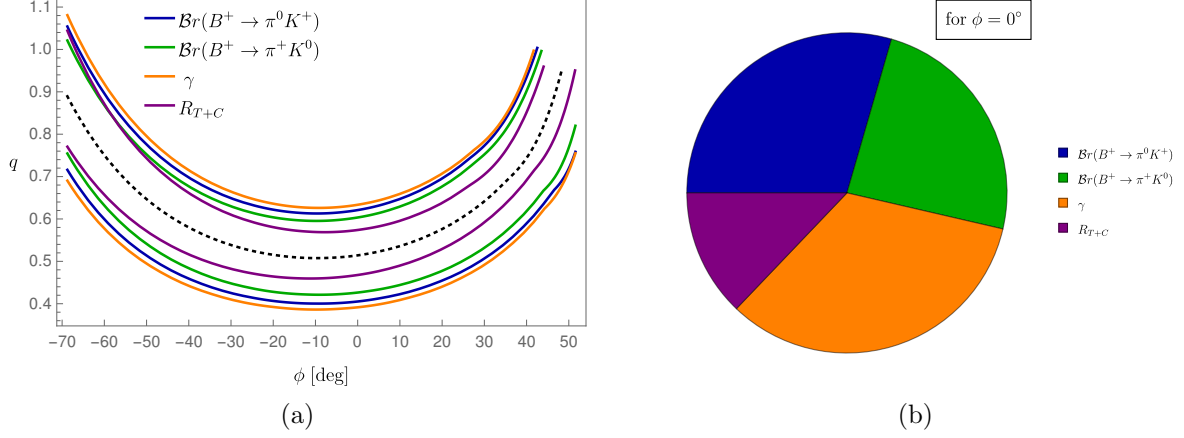


Figure 12: Error budget for the isospin contour in the ϕ - q plane that is consistent with the R_c constraint in Eq. (134): (a) impact of the various parameters when varying them individually within their 1σ ranges; (b) pie chart to illustrate the relative contributions of the parameters to the total uncertainty of q for $\phi = 0^\circ$.

5.2 Utilizing mixing-induced CP violation in $B_d^0 \rightarrow \pi^0 K_S$

In order to not just constrain q and ϕ but to determine these parameters, further information is needed. It is provided by the mixing-induced CP asymmetry $S_{\text{CP}}^{\pi^0 K_S}$, which allows the extraction of the phase ϕ_{00} . If we use the values of the hadronic parameters r_c , δ_c and r , δ as determined in Subsection 3.2, we may convert this observable into a contour in the ϕ - q plane with the help of the following expression:

$$q = \frac{-B_c + \sqrt{B_c^2 - 4A_c D_c}}{2A_c}, \quad (138)$$

where

$$A_c \equiv r_c^2 (-\tan \phi_{00} \cos 2\phi - \sin 2\phi), \quad (139)$$

$$B_c \equiv 2r_c \cos \delta_c (\tan \phi_{00} \cos \phi + \sin \phi) - \frac{4}{3} \hat{c}_+ A_c - (2r_c^2 - 2r_c r \cos(\delta_c - \delta)) (-\tan \phi_{00} \cos(\gamma + \phi) - \sin(\gamma + \phi)) \quad (140)$$

$$D_c \equiv -\tan \phi_{00} - (2r_c \cos \delta_c - 2r \cos \delta) (\tan \phi_{00} \cos \gamma + \sin \gamma) + (r_c^2 + r^2 - 2r_c r \cos(\delta_c - \delta)) (-\tan \phi_{00} \cos 2\gamma - \sin 2\gamma) + \frac{4}{3} \tilde{a}_C q r_c (-\tan \phi_{00} \cos \phi - \sin \phi) + \frac{4}{9} q^2 (\tilde{a}_S^2 + \tilde{a}_C^2) A_c + \frac{4}{3} (-\tan \phi_{00} \cos(\gamma + \phi) - \sin(\gamma + \phi)) (r_c^2 \hat{c}_+ - r_c r (\tilde{a}_C \cos \delta + \tilde{a}_S \sin \delta)) \quad (141)$$

with

$$\hat{c}_+ \equiv \tilde{a}_C q \cos \delta_c + \tilde{a}_S q \sin \delta_c. \quad (142)$$

As discussed in Subsection 3.3.2, we can determine the colour-suppressed EW penguin parameters \tilde{a}_C and \tilde{a}_S in Eqs. (76) and (78) from experimental data using R and $A_{\text{CP}}^{\pi^- K^+}$, allowing us to take also these contributions into account.

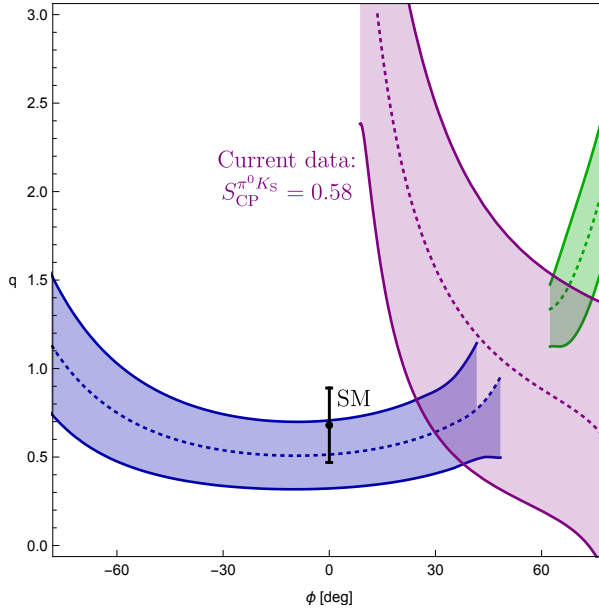


Figure 13: Constraints on the EW penguin parameters q and ϕ from current data. The blue and green contours follow from the isospin analysis and are in agreement with the constraint from R_c .

Scenario	$S_{\text{CP}}^{\pi^0 K_S}$	$A_{\text{CP}}^{\pi^0 K_S}$	ϕ_{00}
1	0.67 ± 0.042	-0.07 ± 0.042	$(0.9 \pm 3.3)^\circ$
2	0.33 ± 0.042	-0.06 ± 0.042	$(23.9 \pm 2.6)^\circ$
3	0.91 ± 0.042	-0.07 ± 0.042	$(-23.0 \pm 6.0)^\circ$

Table 6: Scenarios for future measurements of $S_{\text{CP}}^{\pi^0 K_S}$.

Using the current measurement of $S_{\text{CP}}^{\pi^0 K_S}$ in Table 2 gives

$$\phi_{00} = (7.7 \pm 12.1)^\circ, \quad (143)$$

which should be compared with the SM prediction in Eq. (106). From Eq. (138) we then obtain the purple contour in Fig. 13, which includes contributions from colour-suppressed EW penguin topologies. We show also the contours from the isospin analysis that agree with the R_c constraint, and the SM point from Eq. (39).

In order to demonstrate the future application of our strategy, we consider three scenarios for measurements of $S_{\text{CP}}^{\pi^0 K_S}$ as summarized in Table 6. In the corresponding numerical analyses, we include effects of colour-suppressed EW penguin topologies for completeness. We assume that $S_{\text{CP}}^{\pi^0 K_S}$ has the same uncertainty as $A_{\text{CP}}^{\pi^0 K_S}$ and use the corresponding value anticipated for Belle II in Ref. [4]; unfortunately, the mixing-induced CP asymmetry was not considered in this reference. In Fig. 14, we show the constraints in the ϕ - q plane resulting from $S_{\text{CP}}^{\pi^0 K_S}$ and the isospin determination separately for the three scenarios. We also give the SM point corresponding to the value of R_q in Eq. (40). For the constraints following from $S_{\text{CP}}^{\pi^0 K_S}$, we take into account the experimental uncertainties on $A_{\text{CP}}^{\pi^0 K_S}$ and $S_{\text{CP}}^{\pi^0 K_S}$ as given in Table 6. In addition, we take into account the theoretical $SU(3)$ uncertainties for the hadronic parameters that are required to determine q from Eq. (138). We show these experimental and theoretical uncertainties

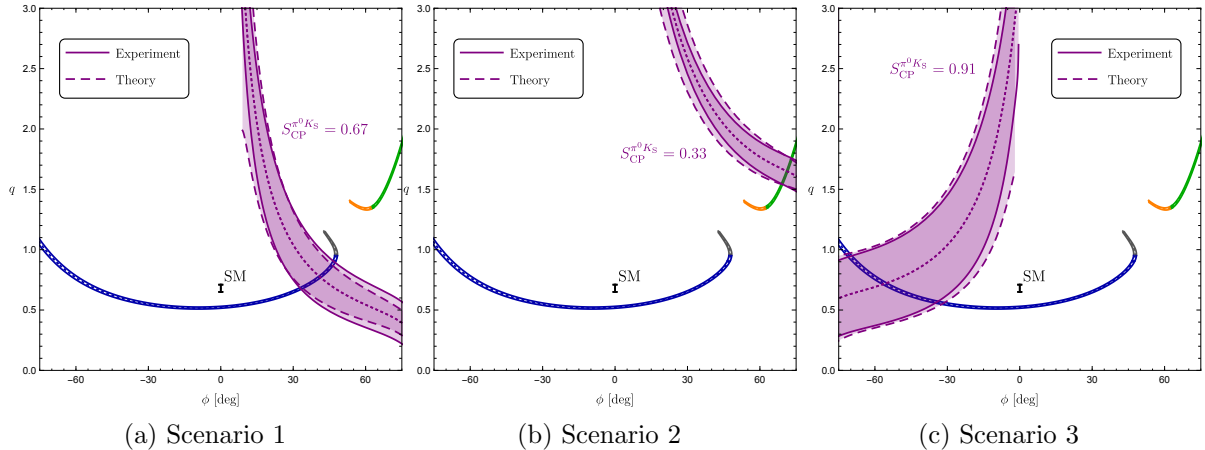


Figure 14: Illustration of the future scenarios specified in Table 6. For the constraints following from measurements of $S_{\text{CP}}^{\pi^0 K_S}$, the experimental and theory uncertainties are given separately.

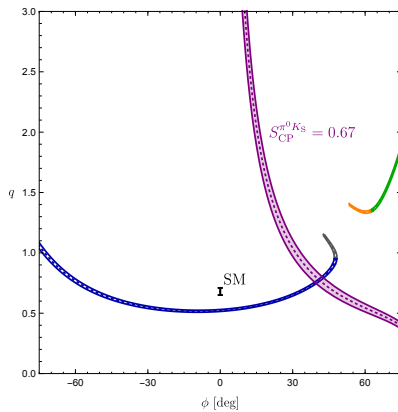


Figure 15: Scenario 1 taking only the expected future theory uncertainties into account.

separately in Fig. 14. In addition, for the isospin triangle constraints we only show the contours that remain after taking into account constraints from ϕ_{0+} and R_c . For the uncertainty, we only consider the uncertainty on R_{T+C} as in Eq. (61). The theory uncertainty (dashed line) matches the future experimental uncertainty (solid line), which is very promising.

Progress on theory and the interplay with experiment may lead to an even sharper picture for the hadronic parameters (see Section 3.2 and Ref. [40]). As an illustration, we assume a scenario where the $SU(3)$ -breaking corrections can be reduced by a factor of four with respect to the current situation. Taking only these uncertainties into account, we obtain the constraints in Fig. 15. These considerations show the exciting potential of the new strategy, going even beyond the next generation of B -decay experiments.

Finally, it is interesting to return to the sum rules discussed in Subsection 3.3.3. The question arises whether they would be significantly affected by the NP scenarios discussed above. In Fig. 16, we show both sum rules as functions of q for several values of ϕ , using the hadronic parameters in Table 3. Here the outer curves correspond to the maximum values that the sum rules can take. The behaviour of $\Delta_{\text{SR}}^{(\text{I})}$ can be easily derived from Eq. (85), i.e. it is linear in q with a slope proportional to $\sin(\gamma - \phi)$. On the other

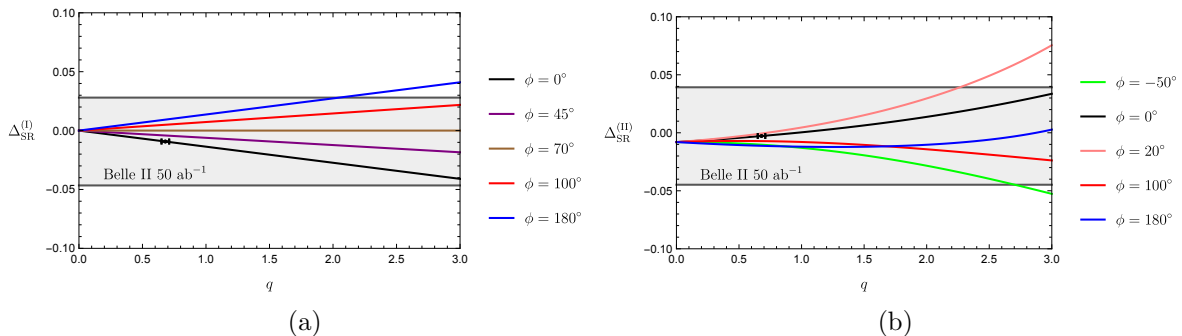


Figure 16: The sum rules introduced in Eqs. (84) and (88) as functions of q for different values of the CP-violating phase ϕ . The grey horizontal band illustrates the ultimate experimental precision at Belle II, assuming an uncertainty of ± 0.042 for $A_{\text{CP}}^{\pi^0 K_S}$ and perfect measurements of the other observables entering the sum rules.

hand, $\Delta_{\text{SR}}^{(\text{II})}$ also depends on q^2 as can be seen from Eq. (89). The grey horizontal bands show the sensitivity of the sum rules at Belle II, assuming an uncertainty for $A_{\text{CP}}^{\pi^0 K_S}$ of ± 0.042 and perfect measurements of the other observables entering Eqs. (84) and (88). The black data point corresponds to the SM values of q and ϕ using R_q in Eq. (40). Consequently, we observe that the experimental resolution would not be sufficient to reveal the NP effects in the EW penguin sector with the sum rules, in contrast to the new method presented above.

6 Conclusions

Employing information on the UT angle γ and the $B_d^0-\bar{B}_d^0$ mixing phase ϕ_d , we use the currently available data for $B \rightarrow \pi\pi$ decays to determine hadronic parameters which characterize these modes and describe the interplay between various tree-diagram-like and penguin topologies. We find agreement with previous studies although our results have higher precision. An important new element in this endeavour is given by measurements of direct CP violation in $B_d^0 \rightarrow \pi^0\pi^0$, allowing us to resolve a twofold ambiguity. The determination of the hadronic $B \rightarrow \pi\pi$ parameters relies only on the isospin symmetry and is hence theoretically clean. Consequently, the corresponding results represent reference values for the comparison with QCD calculations. EW penguin topologies play a negligible role in the $B \rightarrow \pi\pi$ system for the current experimental uncertainties but could be included in the future through more sophisticated analyses.

Utilizing the $SU(3)$ flavour symmetry, we convert the hadronic $B \rightarrow \pi\pi$ parameters into their counterparts in the $B \rightarrow \pi K$ system. We test also the $SU(3)$ flavour symmetry and obtain an impressive global picture which does not indicate any anomalously large non-factorizable $SU(3)$ -breaking corrections. Correspondingly, we do not find indications of an enhancement of colour-suppressed EW penguin topologies when analysing the data. The cleanest SM prediction of the $B \rightarrow \pi K$ observables is a correlation between the direct and mixing-induced CP asymmetries of the $B_d^0 \rightarrow \pi^0 K_S$ decay. As we discussed in detail, it follows from an isospin relation between the neutral $B \rightarrow \pi K$ decay amplitudes and uses the $SU(3)$ flavour symmetry only to fix the magnitude of the $\hat{T}' + \hat{C}'$ amplitude. In comparison with a previous study, a tension of the mixing-induced CP violation in $B_d^0 \rightarrow \pi^0 K_S$ has become more pronounced due to a sharper determination of γ . Moreover,

we have considered the angle ϕ_{\pm} as a new constraint, which also shows tension with respect to the SM. These discrepancies emerging from the current data suggest that either the values of the measured observables will change in the future or indicate NP effects with new sources of CP violation. In the former case, a reduction of the central value of the branching ratio of $B_d^0 \rightarrow \pi^0 K^0$ by about 2.5σ with an increase of the mixing-induced CP asymmetry by about 1σ would give a situation in agreement with the SM. In the latter case, EW penguin topologies offer an attractive avenue for new particles to enter the $B \rightarrow \pi K$ modes.

In view of this intriguing $B \rightarrow \pi K$ puzzle and to test the corresponding sector of the SM, the EW penguin parameters q and ϕ are in the spotlight. We have presented a new strategy to determine these quantities from the data for the neutral and charged $B \rightarrow \pi K$ decays, employing again the corresponding isospin relations. Applying this method to the current data, we already obtain surprisingly stringent constraints in the ϕ - q plane. They are consistent with the SM but leave also a lot of space for possible NP effects. In order to actually pin down ϕ and q further information is needed, which is provided by the mixing-induced CP asymmetry of the $B_d^0 \rightarrow \pi^0 K_S$ decay. Considering a variety of future scenarios, we have illustrated this determination and have shown that the theory uncertainties can match the expected experimental precision in the era of Belle II and the LHCb upgrade. Following these lines, we may determine (q, ϕ) and reveal the dynamics of the $B \rightarrow \pi K$ system with unprecedented accuracy. The resulting picture will either confirm once again the SM or may eventually establish new flavour structures with possible new sources of CP violation.

Acknowledgements

This research has been supported by the Netherlands Organisation for Scientific Research (NWO) and by the Deutsche Forschungsgemeinschaft (DFG), research unit FOR 1873 (QFET).

References

- [1] A. J. Buras and J. Girrbach, Rept. Prog. Phys. **77** (2014) 086201 [arXiv:1306.3775 [hep-ph]].
- [2] N. Cabibbo, Phys. Rev. Lett. **10** (1963) 531.
- [3] M. Kobayashi and T. Maskawa, Prog. Theor. Phys. **49** (1973) 652.
- [4] T. Abe *et al.* [Belle-II Collaboration], arXiv:1011.0352 [physics.ins-det]; T. Aushev *et al.*, arXiv:1002.5012 [hep-ex].
- [5] R. Aaij *et al.* [LHCb Collaboration], Eur. Phys. J. C **73** (2013) 2373 [arXiv:1208.3355 [hep-ex]].
- [6] Y. Nir and H. R. Quinn, Phys. Rev. Lett. **67** (1991) 541.
- [7] M. Gronau, O. F. Hernandez, D. London and J. L. Rosner, Phys. Rev. D **52** (1995) 6374 [hep-ph/9504327].

- [8] M. Gronau, J. L. Rosner and D. London, Phys. Rev. Lett. **73** (1994) 21 [hep-ph/9404282].
- [9] R. Fleischer, Int. J. Mod. Phys. A **12** (1997) 2459 [hep-ph/9612446].
- [10] A. J. Buras and R. Fleischer, Eur. Phys. J. C **11** (1999) 93 [hep-ph/9810260].
- [11] M. Neubert, JHEP **9902** (1999) 014 [hep-ph/9812396].
- [12] M. Beneke and M. Neubert, Nucl. Phys. B **675** (2003) 333 [hep-ph/0308039].
- [13] R. Fleischer, S. Recksiegel and F. Schwab, Eur. Phys. J. C **51** (2007) 55 [hep-ph/0702275 [HEP-PH]].
- [14] M. Gronau and J. L. Rosner, Phys. Lett. B **666** (2008) 467 [arXiv:0807.3080 [hep-ph]].
- [15] C. Bobeth, M. Gorbahn and S. Vickers, Eur. Phys. J. C **75** (2015) 340 [arXiv:1409.3252 [hep-ph]].
- [16] A. J. Buras, R. Fleischer, S. Recksiegel and F. Schwab, Nucl. Phys. B **697** (2004) 133 [hep-ph/0402112].
- [17] A. J. Buras, R. Fleischer, S. Recksiegel and F. Schwab, Phys. Rev. Lett. **92** (2004) 101804 [hep-ph/0312259].
- [18] V. Barger, L. Everett, J. Jiang, P. Langacker, T. Liu and C. Wagner, Phys. Rev. D **80** (2009) 055008 [arXiv:0902.4507 [hep-ph]].
- [19] V. Barger, L. L. Everett, J. Jiang, P. Langacker, T. Liu and C. E. M. Wagner, JHEP **0912** (2009) 048 [arXiv:0906.3745 [hep-ph]].
- [20] R. Fleischer, PoS FPCP **2015** (2015) 002 [arXiv:1509.00601 [hep-ph]].
- [21] N. B. Beaudry, A. Datta, D. London, A. Rashed and J. S. Roux, JHEP **1801** (2018) 074 [arXiv:1709.07142 [hep-ph]].
- [22] W. Altmannshofer, C. Niehoff, P. Stangl and D. M. Straub, Eur. Phys. J. C **77** (2017) 377 [arXiv:1703.09189 [hep-ph]].
- [23] R. Fleischer, Phys. Lett. B **365** (1996) 399 [hep-ph/9509204].
- [24] R. Fleischer, S. Jäger, D. Pirjol and J. Zupan, Phys. Rev. D **78** (2008) 111501 [arXiv:0806.2900 [hep-ph]].
- [25] R. Fleischer, R. Jaarsma and K. K. Vos, arXiv:1712.02323 [hep-ph].
- [26] R. Fleischer, R. Jaarsma, E. Malami and K. K. Vos, arXiv:1805.06705 [hep-ph]; talk given at Rencontres de Moriond 2018, QCD and High Energy Interactions, La Thuile, Italy, 17–24 March 2018, to appear in the Proceedings.
- [27] M. Gronau and D. London, Phys. Rev. Lett. **65** (1990) 3381.
- [28] C. Patrignani *et al.* [Particle Data Group], Chin. Phys. C **40** (2016) 100001.

- [29] Y. Amhis *et al.* [Heavy Flavor Averaging Group (HFAG)], arXiv:1412.7515 [hep-ex]. for updates, see <http://www.slac.stanford.edu/xorg/hfag/>.
- [30] J. P. Lees *et al.* [BaBar Collaboration], Phys. Rev. D **87** (2013) 052009 [arXiv:1206.3525 [hep-ex]].
- [31] T. Julius *et al.* [Belle Collaboration], Phys. Rev. D **96** (2017) 032007 [arXiv:1705.02083 [hep-ex]].
- [32] R. Aaij *et al.* [LHCb Collaboration], arXiv:1805.06759 [hep-ex].
- [33] L. Wolfenstein, Phys. Rev. Lett. **51** (1983) 1945.
- [34] A. J. Buras, M. E. Lautenbacher and G. Ostermaier, Phys. Rev. D **50** (1994) 3433 [hep-ph/9403384].
- [35] J. Charles *et al.*, Phys. Rev. D **91** (2015) 073007 [arXiv:1501.05013 [hep-ph]]; for updates, see <http://ckmfitter.in2p3.fr>.
- [36] M. Gronau and D. Wyler, Phys. Lett. B **265** (1991) 172.
- [37] D. Atwood, I. Dunietz and A. Soni, Phys. Rev. Lett. **78** (1997) 3257 [hep-ph/9612433]; Phys. Rev. D **63** (2001) 036005 [hep-ph/0008090].
- [38] R. Fleischer and S. Ricciardi, proceedings of the 6th International Workshop on the CKM Unitarity Triangle (CKM 2010) [arXiv:1104.4029 [hep-ph]].
- [39] A. Bevan *et al.*, arXiv:1411.7233 [hep-ph]; for updates, see <http://www.utfit.org>.
- [40] R. Fleischer, R. Jaarsma and K. K. Vos, JHEP **1703** (2017) 055 [arXiv:1612.07342 [hep-ph]].
- [41] R. Fleischer, R. Jaarsma and K. K. Vos, Phys. Rev. D **94** (2016) no.11, 113014 [arXiv:1608.00901 [hep-ph]].
- [42] M. Gronau, D. Pirjol and T. M. Yan, Phys. Rev. D **60** (1999) 034021 Erratum: [Phys. Rev. D **69** (2004) 119901] [hep-ph/9810482].
- [43] R. Fleischer, Phys. Rept. **370** (2002) 537 [hep-ph/0207108].
- [44] K. De Bruyn and R. Fleischer, JHEP **1503** (2015) 145 [arXiv:1412.6834 [hep-ph]].
- [45] M. Beneke, G. Buchalla, M. Neubert and C. T. Sachrajda, Nucl. Phys. B **606** (2001) 245 [hep-ph/0104110].
- [46] M. Neubert and J. L. Rosner, Phys. Rev. Lett. **81** (1998) 5076 [hep-ph/9809311]; Phys. Lett. B **441** (1998) 403 [hep-ph/9808493].
- [47] R. Aaij *et al.* [LHCb Collaboration], Phys. Rev. Lett. **118** (2017) 081801 [arXiv:1610.08288 [hep-ex]].
- [48] J. L. Rosner, S. Stone and R. S. Van de Water, [arXiv:1509.02220 [hep-ph]].
- [49] A. Khodjamirian, T. Mannel and M. Melcher, Phys. Rev. D **68** (2003) 114007 [hep-ph/0308297].

- [50] R. Fleischer and T. Mannel, Phys. Rev. D **57**, 2752 (1998) [hep-ph/9704423].
- [51] M. Gronau, Phys. Lett. B **627** (2005) 82 [hep-ph/0508047].
- [52] M. Gronau and J. L. Rosner, Phys. Rev. D **74** (2006) 057503 [hep-ph/0608040].
- [53] B. Aubert *et al.* [BaBar Collaboration], Phys. Rev. D **79** (2009) 052003 [arXiv:0809.1174 [hep-ex]].
- [54] M. Fujikawa *et al.* [Belle Collaboration], Phys. Rev. D **81** (2010) 011101 [arXiv:0809.4366 [hep-ex]].
- [55] S. Faller, R. Fleischer and T. Mannel, Phys. Rev. D **79** (2009) 014005 [arXiv:0810.4248 [hep-ph]].